University of Louisville
ThinkIR: The University of Louisville's Institutional Repository

Electronic Theses and Dissertations

5-2007

DXA measurements using a micro computed tomograph system.

James Bryant May 1981-
University of Louisville

Follow this and additional works at: https://ir.library.louisville.edu/etd

Recommended Citation
May, James Bryant 1981-, "DXA measurements using a micro computed tomograph system." (2007). *Electronic Theses and Dissertations.* Paper 928.
https://doi.org/10.18297/etd/928

This Master's Thesis is brought to you for free and open access by ThinkIR: The University of Louisville's Institutional Repository. It has been accepted for inclusion in Electronic Theses and Dissertations by an authorized administrator of ThinkIR: The University of Louisville's Institutional Repository. This title appears here courtesy of the author, who has retained all other copyrights. For more information, please contact thinkir@louisville.edu.

DXA Measurements Using a Micro Computed Tomograph System

By
James Bryant May
B.S., University of Louisville, 2005

A Thesis
Submitted to the Faculty of the University of Louisville
Speed Scientific School
As Partial Fulfillment of the Requirements
For the Professional Degree

MASTER OF ENGINEERING

Department of Mechanical Engineering

April 2007

DXA Measurements Using a Micro Computed Tomograph System

Submitted by: _____
James Bryant May

A Thesis Approved on

_____
(Date)

by the Following Reading and Examination Committee

_____
Dr. William P. Hnat, Thesis Director

_____
Dr. Michael J. Voor

_____
Dr. John F. Naber

ACKNOWLEDEMENTS

I would like to thank Dr. Hnat and Dr. Voor for offering me this great thesis opportunity and for their guidance and expertise. I would also like to thank Seid Waddel, Yang Shoo and Robert Burden for their assistance with many tasks involved in this project. A special thanks to Roxanne at Nortons for use of the DXA machine and all the people from Hologic for their assistance.

I would also like to thank God, my parents, my family, my fiancé Lindsay and my friends for supporting me throughout life and helping me make it to where I am today. Without them, none of this was possible.

ABSTRACT

The field of bone densitometry has grown rapidly, particularly in the past 15 years. Many techniques are now available from which the physician may choose. The focus of this research is on Dual-Energy X-Ray Absorptiometry (DXA) and Quantitative Computed Tomography (QCT). The basic principle involving DXA is the ability to quantify the degree of attenuation of an energy beam after passage through bone and soft tissue. The X-ray tubes used with DXA narrow the energy beam to produce two distinct photoelectric peaks necessary to separate bone from soft tissue.

Although QCT is a photon absorptiometric technique like DXA, it is unique in that it provides a three-dimensional image, which makes possible a direct measurement of density, and a spatial separation of trabecular from cortical bone.

In this paper, a rabbit and pig femur were scanned using a DXA and QCT scanner. The purpose was to achieve matching results in g/cm^2 from each scanner. Similar sections of interest were taken during each scan for calculation. The QCT grayscale values were then put into a series of formulas to replicate DXA results.

TABLE OF CONTENTS

APPROVAL PAGE....ii

ACKNOWLEDMENTS....iii

ABSTRACT.... iv

LIST OF TABLES.... vii

LIST OF FIGURES ix

I. INTRODUCTION 1

A. Background Information....1
B. Objectives and Scope....3

II. LITERATURE REVIEW 4

III. INSTRUMENTATION AND EQUIPMENT....9

A. Test Specimens 9
B. The DXA System....10
C. The CT System – Physical Basis 11
D. The CT System – Apparatus....12
E. Phantoms in experimentation for CT....13

IV. PROCEDURE....14

A. DXA Scans of Test Specimens....14
B. Digital X-ray Scans of the Pig Femur Specimen #1....16
C. Digital X-ray Scans of the Pig Femur Specimen #2 for Reliability Tests....18
D. Cutting the Pig Femur Specimen #2 in half....21
E. Digital X-ray Scans on the Distal End of the Pig Femur Specimen #2....23
F. Equations for DXA results using the CT Scanner....24
G. Converting DXA results for various manufacturers....27

V. RESULTS AND DISCUSSION....28

A. DXA Scans....28
B. Digital X-ray Scans on the Pig Femur Specimen #1....29
C. Digital X-ray and DXA Scans of the Pig Femur

Specimen #2 for Reliability Tests....32
D. Digital X-ray results with the Pig Femur Specimen #2 in half....34
E. Digital X-ray and DXA calculations on the Distal End of the Pig Femur Specimen #2....36
F. Converting DXA Scan Manufacturers Results....38

VI. CONCLUSIONS....40

A. DXA Scans....40
B. Digital X-ray Scans on the Pig Femur Specimen #1....40
C. Digital X-ray and DXA Scans of the Pig Femur Specimen #2 for Reliability Tests....40
D. Digital X-ray results with the Pig Femur Specimen #2 in half....41
E. Digital X-ray and DXA calculations on the Distal End of the Pig Femur Specimen #2....41
F. Converting DXA Scan Manufacturers Results....41

VII. RECOMMENDATIONS....42

VIII. REFERENCES....43

IX. APPENDIX....44

X. VITA....76

LIST OF TABLES

TABLE I. Instruments and QCT scanner model and manufacturer.....13

TABLE II. Regions pixel height, width and number of pixels for the pig femur specimen #1.....18

TABLE III. Regions pixel height, width and area for the pig femur specimen #2 21

TABLE IV. Region's pixel height, width, and area for the pig femur specimen #2 cut in half.....23

TABLE V. Region's pixel height, width and area for the pig femur specimen #2 distal end 24

TABLE VI. Conversion formulas for BMD in proximal femur between DXA devices.....27

TABLE VII. Conversion formulas for the BMD in the AP spine between DXA devices.....27

TABLE VIII. Regions used in comparison with QCT results for proximal pig femur specimen #1.....28

TABLE IX. The k values for each region used for calculation 30

TABLE X. QCT and DXA BMD calculations and differences for each region of specimen #1 using plaster phantom 30

TABLE XI. QCT and DXA BMD calculations and differences for specimen #2 on day 1 using plaster phantom 31

TABLE XII. QCT and DXA BMD calculations and differences for specimen #2 on day 2 using both phantoms 32

TABLE XIII. QCT and DXA BMD calculations and differences for specimen #2 on day 3 using both phantoms 32

TABLE XIV. The BMD differences between each day for the QCT results using both phantoms.....33

TABLE XV. The area of interest, hi and low BMD difference between each day for the DXA results....33

TABLE XVI. QCT BMD calculations with whole specimen DXA BMD calculations and differences for specimen #2 cut in half using the both phantoms 35

TABLE XVII. QCT BMD calculations with differences between a whole and half pig femur specimen #2 using the both phantoms on each day… ..35

TABLE XVIII. QCT BMD calculations with whole specimen DXA BMD calculations and differences of the distal end for specimen #2 using the both phantoms 37

TABLE XIX. The BMD, difference and % difference for each DXA manufacturer compared to Hologic DXA results and calculated DXA results from a QCT scanner using formulas from Table VI & VII....39

LIST OF FIGURES

FIGURE 1 - Hologic QDR 1000 scanner, a DXA pencil-beam absorptiometer 2

FIGURE 2 - Pencil-beam DXA absorptiometers. The detector and highly collimated X-ray beam move in tandem in a rectilinear path 2

FIGURE 3 - Calculated entry and exit spectra for the X-ray bone densitometer. Exit spectrem reflects attenuation through 20 cm of water 6

FIGURE 4 - Proximal side of the pig femur specimen #1 9

FIGURE 5 - Pig femur specimen #2 with sides labeled accordingly 10

FIGURE 6 - Hologic QDR 4500 DXA 11

FIGURE 7 - Plaster in a wooden cutout, a plexiglass and aluminum sheet to be placed on the intensifier 14

FIGURE 8 - Hologic QDR 4500 X-ray Bone Densitometer 15

FIGURE 9 - Pig femur specimen #1 in a plastic bag with a sheet of plexiglass placed on the intensifier 16

FIGURE 10 - 1st region selected from QCT images for calculations for the pig femur specimen #1 17

FIGURE 11 - 2nd region selected from QCT images for calculations for the pig femur specimen #1 17

FIGURE 12 - 3rd region selected from QCT images for calculations for the pig femur specimen #1 18

FIGURE 13 - The pig femur specimen #2 placed in the QCT scanner against the intensifier 19

FIGURE 14 - Region selected from repeatability test on the first day 20

FIGURE 15 - Region selected from repeatability test on the second day 20

FIGURE 16 - Region selected from repeatability test on the third day 21

FIGURE 17 - The pig femur specimen #2 was cut in half at the proximal end 22

FIGURE 18 - The inside of the halves of the proximal end of the pig femur specimen #2 22

FIGURE 19 - The proximal end of the pig femur specimen #2 set up with an aluminum sheet on the intensifier 23

FIGURE 20 - Region selected from the distal end of the bone for calculation 24

FIGURE 21 - Q scan plot 26

FIGURE 22 - DXA results from pig femur specimen #1 42

FIGURE 23 - DXA results from pig femur specimen #2 on day 1 42

FIGURE 24 - DXA results from pig femur specimen #2 on day 2 43

FIGURE 25 - DXA results from pig femur specimen #2 on day 3 43

FIGURE 26 - DXA results from distal end of the pig femur specimen #2 43

FIGURE 27 - Histogram of the 1st region air scan for the pig femur specimen #1 45

FIGURE 28 - 1st region air scans 45

FIGURE 29 - The “bone” points for air 45

FIGURE 30 - Histogram of the 1st region plaster scan for the pig femur specimen #1 46

FIGURE 31 - 1st region plaster scans 46

FIGURE 32 - The “bone” points for plaster 46

FIGURE 33 - Histogram of the 1st region plexiglass scan for the pig femur specimen #1 47

FIGURE 34 - 1st region plexiglass scans 47

FIGURE 35 - The “bone” points for plexiglass 47

FIGURE 36 - Histogram of the 2nd region air scan for the pig femur specimen #1 48

FIGURE 37 - 2nd region air scans 48

FIGURE 38 - The “bone” points for air.....48

FIGURE 39 - Histogram of the 2nd region plaster scan for the pig femur specimen #1 49

FIGURE 40 - 2nd region plaster scans.....49

FIGURE 41 - The “bone” points for plaster.....49

FIGURE 42 - Histogram of the 2nd region plexiglass scan for the pig femur specimen #1 50

FIGURE 43 - 2nd region plexiglass scans.....50

FIGURE 44 - The “bone” points for plexiglass.....50

FIGURE 45 - Histogram of the 3rd region air scan for the pig femur specimen #1 51

FIGURE 46 - 3rd region air scans 51

FIGURE 47 - The “bone” points for air.....51

FIGURE 48 - Histogram of the 3rd region plaster scan for the pig femur specimen #1 52

FIGURE 49 - 3rd region plaster scans.....52

FIGURE 50 - The “bone” points for plaster.....52

FIGURE 51 - Histogram of the 3rd region plexiglass scan for the pig femur specimen #1 53

FIGURE 52 - 3rd region plexiglass scans.....53

FIGURE 53 - The “bone” points for plexiglass.....53

FIGURE 54 - Histogram of the 1st day region air scan for the pig femur specimen #2 54

FIGURE 55 - Histogram of the 1st day region aluminum scan for the pig femur specimen #2 55

FIGURE 56 - Histogram of the 1st day region plexiglass scan for the pig femur specimen #2 56

FIGURE 57 - Histogram of the 1st day region plaster scan for the pig femur specimen #2 57

FIGURE 58 - Histogram of the 2nd day region air scan for the pig femur specimen #2 58

FIGURE 59 - Histogram of the 2nd day region aluminum scan for the pig femur specimen #2 59

FIGURE 60 - Histogram of the 2nd day region plexiglass scan for the pig femur specimen #2 60

FIGURE 61 - Histogram of the 2nd day region plaster scan for the pig femur specimen #2 61

FIGURE 62 - Histogram of the 3rd day region air scan for the pig femur specimen #2 62

FIGURE 63 - Histogram of the 3rd day region aluminum scan for the pig femur specimen #2 63

FIGURE 64 - Histogram of the 3rd day region plexiglass scan for the pig femur specimen #2 64

FIGURE 65 - Histogram of the 3rd day region plaster scan for the pig femur specimen #2 65

FIGURE 66 - Histogram of the proximal region air scan for the pig femur specimen #2 cut in half 66

FIGURE 67 - Histogram of the proximal region aluminum scan for the pig femur specimen #2 cut in half 67

FIGURE 68 - Histogram of the proximal region plexiglass scan for the pig femur specimen #2 cut in half 68

FIGURE 69 - Histogram of the proximal region plaster scan for the pig femur specimen #2 cut in half 69

FIGURE 70 - Histogram of the distal end region air scan for the pig femur specimen #2 70

FIGURE 71 - Histogram of the distal end region aluminum scan for the pig femur specimen #2 71

FIGURE 72 - Histogram of the distal end region plexiglass scan for the pig femur specimen #2 72

FIGURE 73 - Histogram of the distal end region plaster scan for the pig femur specimen #2 73

I. INTRODUCTION

A. Background Information

The ability to quantify the degree of attenuation of a photon energy beam after passage through bone and soft tissue is referred as dual-energy X-ray aborptiometry (DXA). DXA uses an X-ray tube, which has several advantages in experimentation. There is no replacement of the radioactive source due to source decay or drift in patient values. The X-ray tube will produce greater photon flux with a smaller focal-spot that allows for better beam collimation. Better beam collimation results in less dose overlap between scan lines and greater image resolution with faster scan times and improved precision.

X-ray tubes produce a wide range of photon energies in a single beam. The beam, because of this, must be narrowed in order to produce the two distinct photo electric peaks necessary to separate bone from soft tissue. There are three major manufacturers of dual-energy X-ray absorptiometers in the United States, all with different methods of experiment. Lunar Corp. of Madison, WI, and Norland Medical Systems, Inc. of Fort Atkinson, WI, use rare earth K-edge filters to produce two distinct photoelectric peaks. The Hologic DXA employs alternating pulses to the X-ray source between 70 and 140kV.[1] The Hologic QDR 1000 scanner, a DXA pencil-beam absorptiometer is shown in Figure 1. Figure 2 shows the detector and highly collimated X-ray beam move in tandem in a rectilinear path.

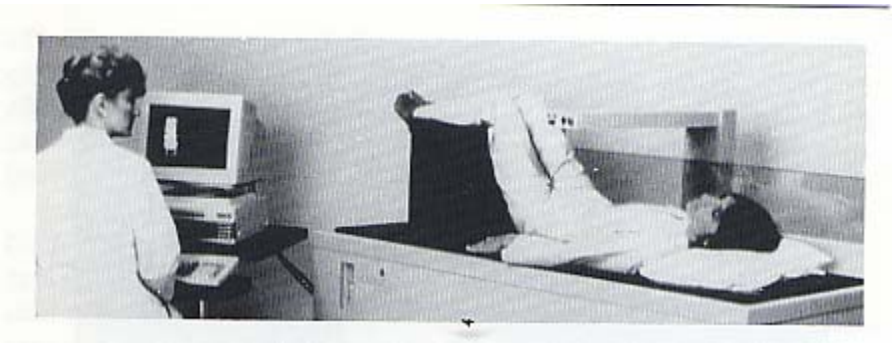

Figure 1. Hologic QDR 1000 scanner, a DXA pencil-beam absorptiometer.[1]

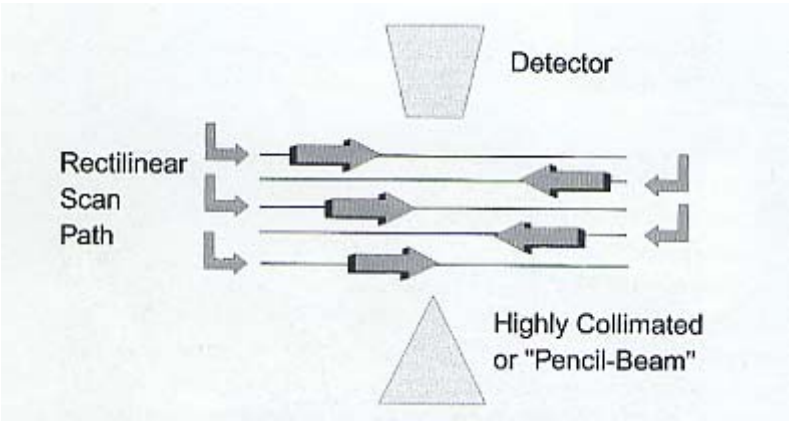

Figure 2. Pencil-beam DXA absorptiometers. The detector and highly collimated X-ray beam move in tandem in a rectilinear path. [1]

The quantitative computed tomography (QCT) is a photon absorptiometric technique like dual photon absorption (DPA) and DXA, and is unique in that it provides a three-dimensional image, which makes possible a direct measurement of density, and a spatial separation of trabecular from cortical bone. QCT studies of the spine utilize a reference standard or phantom, which is scanned simultaneously with the patient. The phantom, which contains varying concentrations of K_2HPO_4, is placed underneath the patient during the study. A scout view is required for localization, and then an 8-10-mm-thick slice is measured through the center of two or more vertebral bodies, which are generally selected from T12 to L3. A region of interest within the anterior portion of the vertebral body is analyzed for bone density, and is reported as mg/cm^3 K_2HPO_4 equivalents. This region of interest is carefully placed to avoid the cortical shell of the

vertebral body. The result is a three-dimensional trabecular density, unlike the two-dimensional areal mixed cortical and trabecular densities reported with anterior-posterior studies of the spine utilizing DPA or DXA.

A study of the spine with QCT requires about 30 minutes with a skin-radiation dose generally around 100-300 mrem.[3] Only a small portion of marrow is irradiated during a QCT study of the spine making the overestimations of the effective radiation dose important. The effective dose, or whole-body equivalent dose, is generally in the range of only 3 mrem. The localizer scan that preceded the actual QCT study will add an additional 3 mrem to the effective dose. Compared to the natural background radiation of approximately 20 mrem per month, these values are still quite acceptable. QCT units deliver skin and absorbed doses 3-10-x higher, which is by their design to be unable to utilize low kVp settings for QCT studies.[3]

QCT of the spine has been used in studies of prevalent osteoporotic fractures, and can distinguish osteoporotic individuals better than DPA. Fractures are rare with values above 110 mg/cm^3 and extremely common below 60 mg/cm^3.[3] QCT measures only trabecular bone, which is more metabolically active than cortical bone, which makes QCT spine measurements produce a greater magnitude than those observed with anterior-posterior spine studies performed with DXA or DPA.

B. Objectives and Scopes

The scope of this study is to compose a method of calibration so that a QCT may be used to calculate DXA bone mineral density measurements. This is accomplished through a series of scans with tissue and bone-like phantoms. The output data results in

arrays of grayscale values. From the output data, the grayscale values are put into a series of equations where bone points are then separated from tissue points by choosing a threshold from a histogram compiled of the "bone" and "non-bone" points. The bone mineral density is then calculated from a ratio of "bone" points multiplied by a bone-like density used in one of the phantoms. The digital X-ray and DXA results are compared and repeatability is tested. The objectives for this research are:

- To find materials that can be suitable for use as tissue and bone-like phantoms.
- To compare other materials of different densities to see if similar results can be achieved.
- To develop a method of calculation and calibration for the digital X-ray so that it may be used to achieve DXA bone mineral density measurements.
- To compare data from DXA and digital X-ray calculations for similarity, repeatability and exposure to different conditions involving energy levels, denser phantoms, and different areas of interest taken for calculation.
- To develop an Excel spreadsheet to easily input arrays of grayscale values from Image J and achieve BMD calculations.

II. LITERATURE REVIEW

A dual-energy bone densitometer, DXA, utilizes an X-ray tube driven by a dual-voltage pulsed power supply as the photon source. This source provides approximately 500-fold more photon flux than the 1-Curie Gadolinium-153 sources typically used in bone mineral analyzers.[4] The flux increase is used to improve scan resolution, reduce imaging time, and improve precision. The system records separate low energy values for patient and reference measurements on a pixel-by-pixel basis. This scheme compensates for power supply and detector variations, adjusts for spectral effects such as hardening of the X-ray beam by patient soft tissues, and obviates the need for periodic external calibration. The system is capable of determining the bone mineral density of the lumbar spine with a five-minute scan time, an entrance exposure of under 3 mrem, and a precision of better than 0.01 g/cm^2.[4]

Assessment of the bone mineral content, BMC, of the axial skeleton is required for diagnosis and treatment of metabolic bone diseases, particularly osteoporosis. Dual-photon absorptiometry, DPA, is a widely-utilized technique to obtain this measurement, though, its utility is impaired by limited precision, which is not adequate to detect an individual patient's bone loss in a reasonable time. DPA examination times of 20-30 minutes are undesirable.[4]

In the X-ray bone densitometer, the photon source is a tungsten stationary-anode X-ray tube, pulsed alternately at 70 kVp (kilovolt peak) to 140 kVp, and operated at a peak tube current of about 3 mA (milliamps).[4] Aluminum half-value-layer measurements were used to determine effective beam energies of 43 keV and 110 keV.[4] The 70 kVp

filteration is 2mm Al, and the 140 kVp filteration employs an additional 1.6 mm brass.[4] Filters are mounted on a wheel which rotates synchronously with the voltage pulsing frequency and which serves as an additional calibration. The photon flux obtained from the X-ray tube is comparable to that which would be obtained from a 500-Curie Gd-153 source.[4] Figure 3 shows the calculated entry and exit spectra for the X-ray bone densitometer.

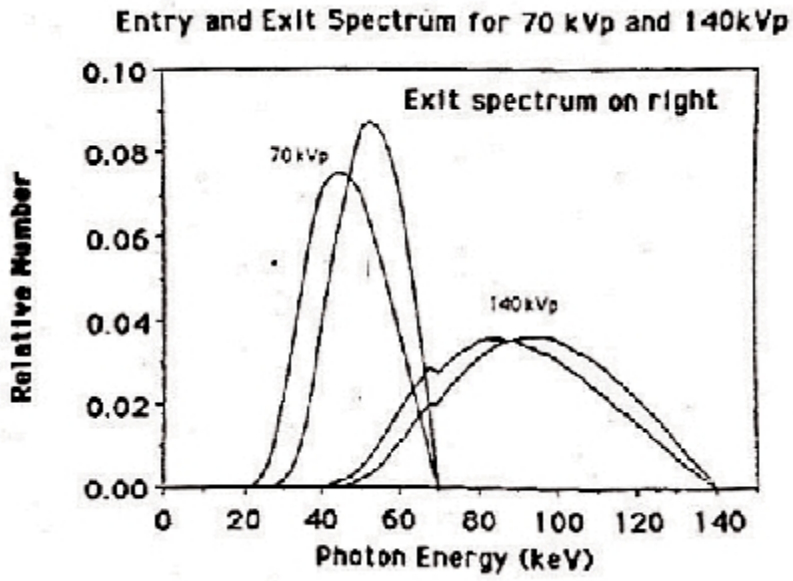

Figure 3. Calculated entry and exit spectra for the X-ray bone densitometer. Exit spectrum reflects attenuation through 20 cm of water.[4]

DXA can access most regions of the skeleton. Studies can be made of the spine in both an anterior-posterior and lateral direction. The lateral projection in the anterior-posterior direction offers the ability to eliminate the confounding effects of dystrophic calcification on densities measured. Lateral scans also eliminate the highly cortical posterior elements, which contribute as much as 47% of the mineral content measured in the anterior-posterior direction.[2] The proximal femur, radius, calcaneus, and total body can also be evaluated with DXA.

Scan times are dramatically shorter with DXA where early units require approximately 4 minutes for studies of the anterior-posterior spine or proximal femur. Total body studies required 20 minutes in the medium-scan mode and only 10 minutes in the fast-scan mode.[2] Present DXA units in studies of the anterior-posterior spine or proximal femur requiring only 2 minutes to perform.[2]

DXA studies of the skeleton are highly correlated with values from earlier studies performed with dual-photon absorption or DPA. DXA spine values, and Hologic DXA proximal femur values, are consistently lower than those obtained with DPA. The Hologic and Norland DXA units are also consistently lower than those obtained with a Lunar DXA unit, although all are highly correlated with each other. Formulas, found in Tables VI and VII, can be used for conversion of values between all three manufacturers' equipment, but a large margin of error in such conversions cannot make such comparisons clinically useful. To eliminate this problem in the future, a standardized bone mineral density or a universal standard to which the machines could be calibrated should be developed.

Radiation exposure with DXA during an anterior-posterior spine or proximal femur study is only 2-5 mrem, which is extremely low for all scan types.[1] The biologically important effective dose, or whole-body equivalent dose, is only 0.1 mrem. So the radiation dose for the body is too low for any major effects and considered irrelevant.

The most significant advance seen with DXA is the marked improvement in precision. Expressed as a coefficient of variation, short-term precision in normal subjects has been reported as low as 0.9% for the anterior-posterior lumbar spine, and 1.4% for

the femoral neck. Precision studies over the course of 1 year have reported values of 1 % for the lumbar spine and 1.7-2.3 % for the femoral neck.[1] DXA has been used in prospective studies to predict fracture risk in different areas of the body.

The accuracy of QCT for measurements of spine BMD is affected by the presence of marrow fat. As the marrow fat increases with age, the accuracy of QCT is reported to range from 5 to 15%, depending on the age of the patient and percentage of marrow fat. marrow fat results in an increasingly large error in the accuracy of spine QCT measurement the older the patient is. The presence of marrow fat results in an underestimation of bone density in the young of about 20 mg/cm^3, and as much as 30 mg/cm^3 in the elderly.[3] In an attempt to eliminate the error introduced by the presence of marrow fat, to as low as 1.4% in cadaveric studies, data is applied on vertebral marrow fat with aging.[3] The cost of a QCT spinal bone density measurement is around $150.[3]

The ability to measure bone density in the proximal femur with QCT is also limited. Using both dedicated QCT and standard units, investigators have attempted to utilize QCT for measurements of the proximal femur. This capability remains restricted to a few research centers.

III. INSTRUMENTATION AND EQUIPMENT

A. Test Specimens

Two separate left pig femurs were used in testing. The names are labeled pig femur specimen #1 and pig femur specimen #2, respectively. Figure 4 shows the proximal side of pig femur specimen #1 that was used for the first of the two experiments performed. Pig femur specimen #2 was tested on both the promixal and distal sides of the bone. Figure 5 shows the pig femur specimen #2 with both sides labeled accordingly. Both specimens were taken from the medical school's bioengineering lab at the University of Louisville. Both are left femur bones with similar dimensions.

Figure 4. Proximal side of the pig femur specimen #1.

Figure 5. Pig femur specimen #2 with sides labeled accordingly.

B. The DXA System

The DXA system produces a two-dimensional data output using an X-ray source. An X-ray source, consisting of a generator and tube in a common, shielded enclosure, is mounted beneath the patient and generates a narrow, tightly collimated, fan shaped beam of X-rays which alternate, at power line frequency, between 100 kVp and 140 kVp. At one end of a C-arm is the source while at the other end, above the patient, is a crystal/solid state detector. During a scan, the C-arm and table move under computer control to guide the beam over the desired scan area. Figure 6 shows the Hologic QDR 4500 DXA.

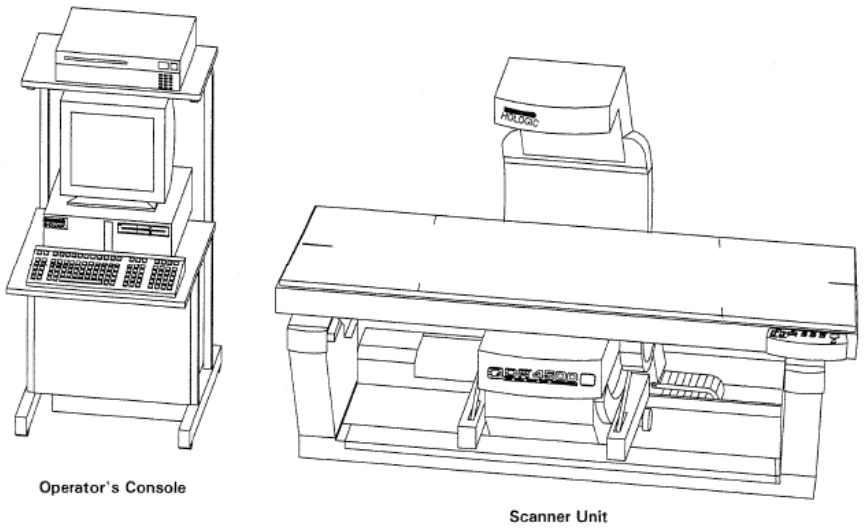

Figure 6. Hologic QDR 4500 DXA.[4]

Before passing through the patient, the beam is filtered through a rotating drum, in which alternating segments have radio-opacities equivalent to tissue, bone and air. When finally intercepted by the detector, the beam contains information about the X-ray absorbing characteristics of both the patient and the calibration materials in the filter drum. An A/D converter, fed by the detector, supplies a complex digital signal to the computer, which uses the signal to both construct the screen display and as the basis for its computations of BMC and BMD.

C. The CT System - Physical Basis

Computed tomography, or CT, is a three-dimensional data output consists of a narrow beam of X-ray scans across the structure to be imaged in linear fashion. A radiation detector detects the nonabsorbed X-rays. While traversing the object, the radiation detector scans synchronously with the beam and is repeated at different angles around the object. The data is acquired in series of profiles that reflect the attenuation

properties of the object scanned at different angles. A transverse tomographic image of the object can then be reconstructed as these profiles are put into a complex mathematical algorithm. The data acquired from CT for the reconstruction of the image have considerably greater number of X-ray photons used per resolution element than in conventional diagnostic radiology. This is due to a better signal-to-noise ratio where the detector in the CT provides less noise than radiographic film.

The CT radiation beam is narrowly collimated, both before entering and after emerging from the patient, which only allows a minimal amount of scattered radiation to reach the detector. This effect causes tissue contrast differentiation capability to be far superior to conventional radiography. CT then uses the filtered back-projection method of image reconstruction that provides images that are recorded in conventional tomography.

D. The CT System - Apparatus

The data is acquired by measuring of the attenuation of the X-radiation passing through the tissue to be imaged. The ability of a CT device to reproduce the morphology of the assessed structures in the reconstructed image is dependant on the number of physical measurements taken. In CT, the X-ray beam images suitable linear and angular sampling frequencies of the object. Data acquisition in the projection of the image along a line perpendicular to the direction of the X-ray beam is reflected in linear sampling frequency. The angular sampling frequency is the number of measurements captured at different angles around the object.

To achieve the proper linear and angular sampling, a large quantity of different motions has been incorporated into CT gantries. For commercially available CT devices, two different configurations are used. The first configuration has a synchronous sequence of rotation with the X-ray tube and the array of detectors. The other configuration uses a stationary detector array while the X-ray tube rotates around the patient. Both of these configurations provide some physical advantage though it is not clear whether one is more superior to the other.

The data, after preliminary mathematical preprocessing, are converted into images from a computer-applied algorithm. The image can be displayed in either analog form as an optical image on a cathode ray oscilloscope or as a digital matrix produced by a line printer. Table I provides each instruments model and manufacturer in experimentation.

TABLE I

INSTRUMENTS AND QCT SCANNER MODEL AND MANUFACTURER

Instrument	Model	Manufacturer
Micro CT Scanner	Actis 225 KV	BioImaging Research
X-Ray System	FXE 225.20	FeinFocus USA, Inc.
Image Intensifier	19466HP	North America Imaging
Camera	1M15	Dalsa

E. Phantoms in experimentation for CT.

To achieve similar results from DXA data in CT data output, certain methodology was used that involved the use of phantoms. Phantoms were placed on the intensifier in the CT scanner, while the images were being taken. This is similar to the DXA procedure where phantoms are placed underneath the table where a specimen would sit while having a DXA scan performed. A bone-like density had to be constructed as well

as a flesh-like density. Plaster has a similar density to bone and was used as a phantom. A piece of plywood was cut into a square and then had another square cut out from it. The plaster was placed in an 8.731 cm by 12.383 cm square cut out of a 0.318 cm piece of wood. The density of the plaster with those dimensions was 41.7 grams. The sheets of plaster and plexiglass, shown in Figure 7, both had a uniform thickness of 0.318 cm. The aluminum sheet, also shown in Figure 7, has a density of 2.635 grams and a uniform thickness of 0.318 cm.

Figure 7. Plaster in a wooden cutout, a plexiglass and aluminum sheet to be placed on the intensifier.

IV. PROCEDURE

A. DXA Scans of test specimens.

The Hologic QDR 4500 X-ray Bone Densitometer, located at the Norton Healthcare Pavilion, was used to scan two left femur bones of a pig. The pig bones were placed in a plastic bag and laid on the table of the DXA machine shown in Figure 8.

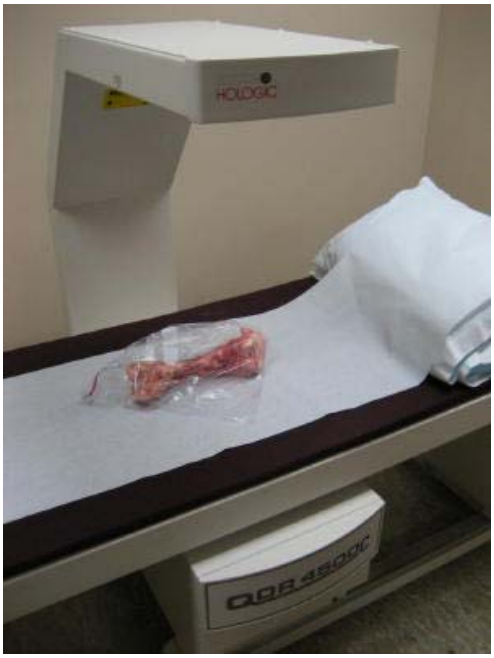

Figure 8. Hologic QDR 4500 X-ray Bone Densitometer.

Sections from the top left of the proximal ends of both specimens were selected for measurement. The area, bone mineral content and bone mass density for sections defined as the neck, troch, and inter were computed. Specimen #2 also had a DXA scan done on the distal end of the femur.

B. Digital X-ray Scans of the Pig Femur Specimen #1.

The pig femur bone was placed in the digital X-ray scanner shown in Figure 9. Three separate scanning procedures were performed. One scan was done with just the bone. The other two had a sheet of plexiglass and a sheet of plaster placed in front of the intensifier. Two different scans at 100 and 140 kVp were taken for each procedure. Figure 9 shows the plexiglass placed on the intensifier.

Figure 9. Pig femur specimen #1 in a plastic bag with a sheet of plexiglass placed on the intensifier.

Figure 10 through 12 shows the 1st, 2nd, and 3rd regions of the bone from the digital X-ray image. The image produces grayscale values for the area, which can be plugged into equations for further calculation. The regions were selected for comparison to the section selected with the DXA scanner. Table II defines the pixel height and width as well as the height, width and area of each region.

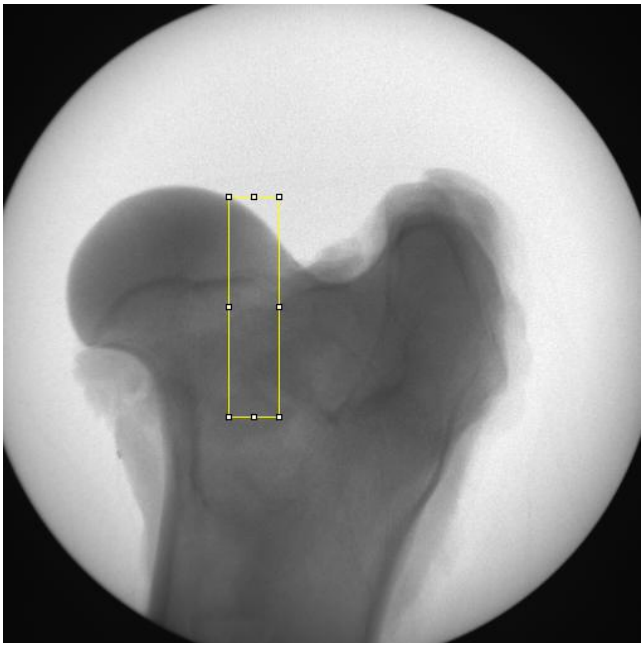

Figure 10. 1st region selected from digital X-ray images taken from the pig femur specimen #1.

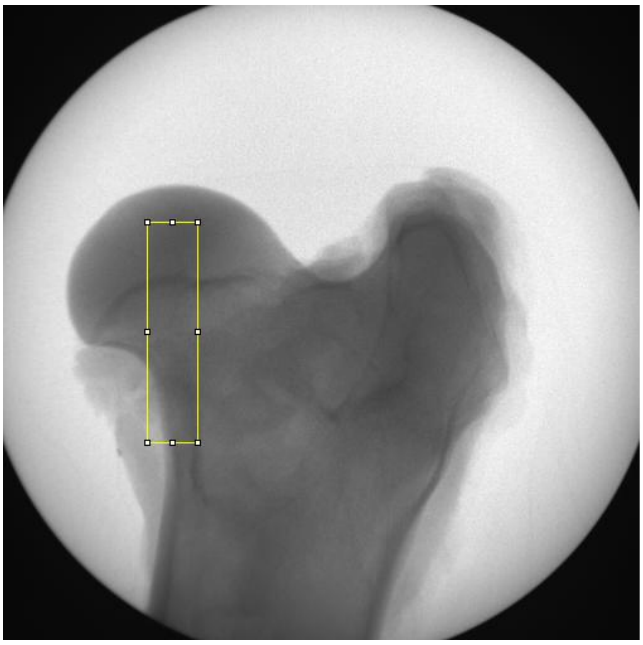

Figure 11. 2nd region selected from digital X-ray images taken from the pig femur specimen #1.

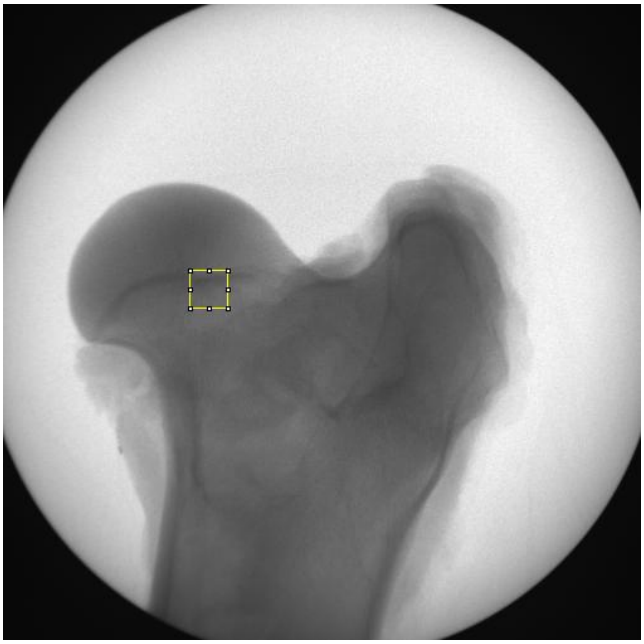

Figure 12. 3rd region selected from digital X-ray images taken from the pig femur specimen #1.

TABLE II

REGIONS PIXEL HEIGHT, WIDTH AND AREA FOR THE PIG FEMUR SPECIMEN #1

	Pixel Height (cm)	Pixel Width (cm)	Height (Number of Pixels)	Width (Number of Pixels)	Area (cm^2)
QCT 1st Region	0.0136914	0.0128906	350	80	4.942
QCT 2nd Region	0.0136914	0.0128906	350	80	4.942
QCT 3rd Region	0.0136914	0.0128906	60	60	0.635

C. Digital X-ray scans of the Pig Femur Specimen #2 for repeatability tests.

A second series of tests were performed on a second left pig femur. The tests included using an aluminum sheet in the digital X-ray scanner as a phantom in addition to the plaster and the plexiglass that were used as phantoms. Figure 13 shows the pig femur specimen #2 placed in the digital X-ray scanner in front of the intensifier. A set of scans

using both digital X-ray and DXA were performed and then repeated on three separate days. The purpose of this test was to check for repeatability.

Figures 14 through 16 show the regions selected for the repeatability tests on each day, respectively. The inexact repeated placements of the femur bone in the digital X-ray each day leads to a slight difference in the region selected each day. The region was selected in a similar placement in the digital X-ray, as the previous days but there is no way to assure it was the exact placement. The regions are selected differently in Figures 14 through 16 because the difference in the BMD isn't significant enough. The regions were selected for comparison to the section selected with the DXA scanner. Table III defines the pixel height and width as well as the height, width and area of each region.

Figure 13. The pig femur specimen #2 placed in the digital X-ray scanner against the intensifier.

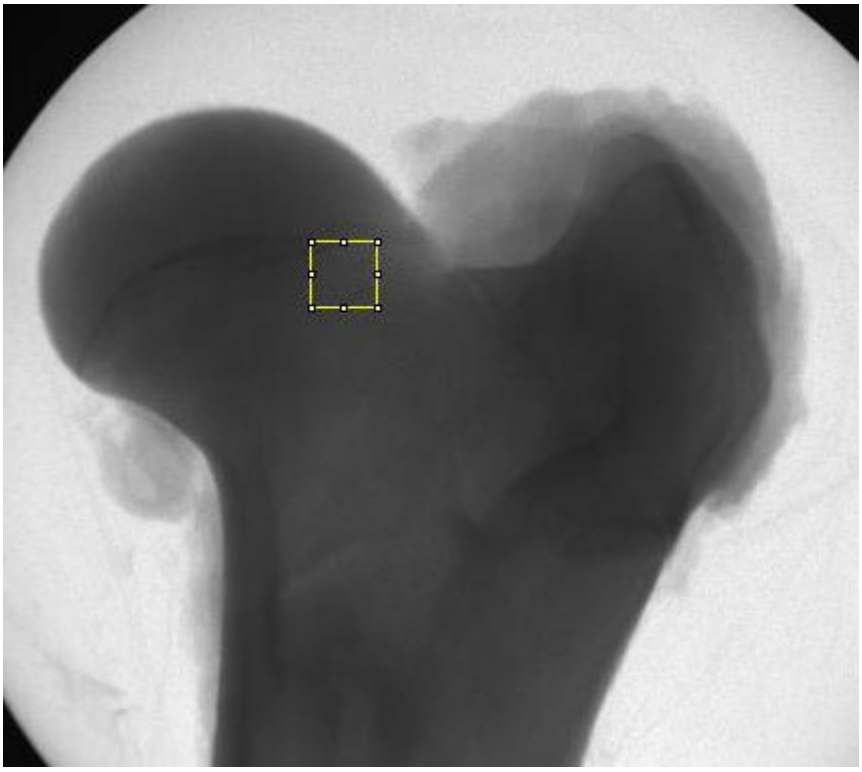

Figure 14. Region selected from repeatability test on the first day.

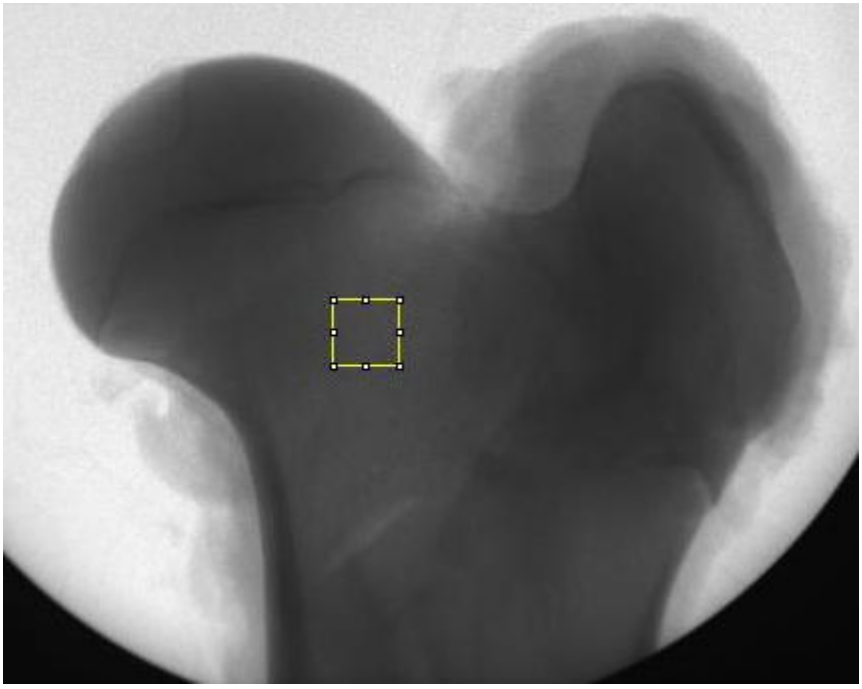

Figure 15. Region selected from repeatability test on the second day.

Figure 16. Region selected from repeatability test on the third day.

TABLE III

REGIONS PIXEL HEIGHT, WIDTH, AND AREA FOR THE PIG FEMUR SPECIMEN #2

	Pixel Height (cm)	Pixel Width (cm)	Height (Number of Pixels)	Width (Number of Pixels)	Area (cm^2)
CT 1st Day Region	0.0136914	0.0128906	66	66	0.769
CT 2nd Day Region	0.0136914	0.0128906	66	66	0.769
CT 3rd Day Region	0.0136914	0.0128906	66	66	0.769

D. Cutting the pig femur specimen #2 in half.

Another test performed with pig femur specimen #2 was cutting the bone in half and performing another set of digital X-ray scans. The calculations are compared between the whole bone and half bone to see if similar results in bone mineral density are

produced. Figure 17 shows how the pig femur was cut in half at the proximal end. Figure 18 shows that the inside half of the pig femur bone. Figure 19 shows how the proximal end was set up with an aluminum sheet on the intensifier. Table IV shows the region's pixel height, width and area for the pig femur specimen #2 cut in half.

Figure 17. The pig femur specimen #2 was cut in half at the proximal end.

Figure 18. The inside of the halves of the proximal end of the pig femur specimen #2.

Figure 19. The proximal end of the pig femur specimen #2 set up with an aluminum sheet on the intensifier.

TABLE IV

REGION'S PIXEL HEIGHT, WIDTH AND AREA FOR THE PIG FEMUR SPECIMEN #2 CUT IN HALF.

	Pixel Height (cm)	Pixel Width (cm)	Height (Number of Pixels)	Width (Number of Pixels)	Area (cm^2)
CT Proximal Region	0.0136914	0.0128906	66	66	0.769

E. Digital X-ray scans on the distal end of the pig femur specimen #2.

A set of scans on the distal end of pig femur specimen #2 where grayscale values are produced for calculation. The distal side provided a higher bone mineral density compared to the proximal side. BMD calculations, the same calculations done in previous experimentation, were used to see if similar results could be achieved at a higher BMD at the distal end. The region selected from the distal end of the bone for calculation

is shown in Figure 20. Table V shows the region's pixel height, width and area for the pig femur specimen #2 distal end.

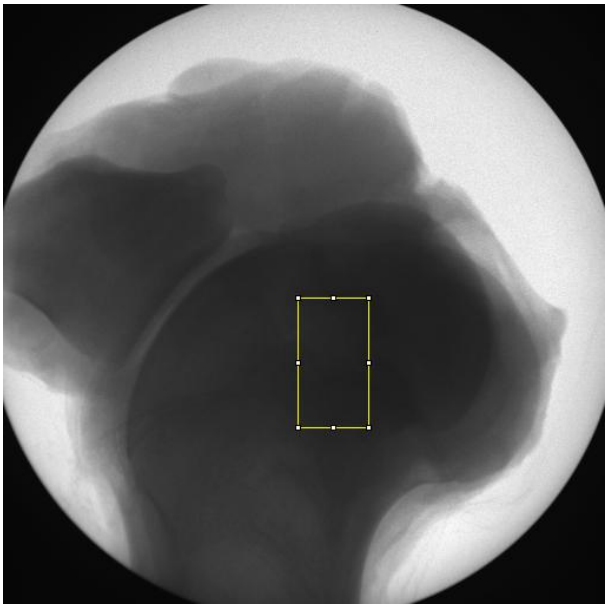

Figure 20. Region selected from the distal end of the bone for calculation.

TABLE V

REGION'S PIXEL HEIGHT, WIDTH AND AREA FOR THE PIG FEMUR SPECIMEN #2 DISTAL END

	Pixel Height (cm)	Pixel Width (cm)	Height (Number of Pixels)	Width (Number of Pixels)	Area (cm^2)
CT Distal Region	0.0136914	0.0128906	220	120	4.659

F. Equations for DXA results using the CT scanner.

The Hologic QDR 4500 computer algorithm is based on the principle that bone attenuates the X-ray beam differently at high and low energies. The bone mineral content of any sample point is computed from

$$Q = L - kH \tag{1}$$

where H and L are logarithms of the sample attenuation at high (140kVp) and low (100kVp) energies, respectively, and the constant k depends on the tissue attenuation characteristics of the beam. In the QDR 4500, k is continuously measured using the "tissue" segment in the filter wheel. The constant k is defined as

$$k = [L_{tissue} - L_{air}]/[H_{tissue} - H_{air}] \quad (2)$$

where H and L are logarithms of the sample attenuation at high (140kVp) and low (100kVp) energies for tissue and air. The subscript "air" designates the filter drum segment, which contains no bone- or tissue-equivalent material.

Using the value of k, Q is calculated for each point scanned using Equation 1. The array of Q values constitutes a "Q scan". A histogram of Q values is then compiled. Because a large portion of the scan contains soft tissue only, this histogram will have a large peak. A threshold value is chosen just beyond this peak, and that value is discriminated, point by point, in the Q scan, between "bone" points and "non-bone" points. The threshold value is theoretically the point where the Q values start representing soft tissue points. Those soft tissue points are then eliminated from further calculations and "bone" points are all that is left for calculation. Figure 4 shows the Q scan plot threshold with the "bone" and "non-bone" points defined.

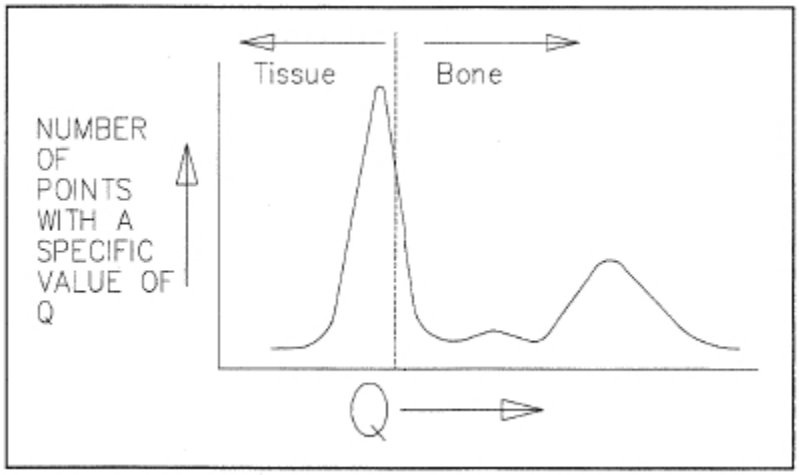

Figure 21. Q scan plot.[5]

Using the "bone" points, a new histogram is formed. The segment boundaries are smoothed to eliminate isolated noise-generated "bone" points. These noise generated "bone points" can cause unexpected spikes in data and are irrelevant to the calculations. The boundaries are smoothed using linear regression in Microsoft Excel, where these calculations were performed. The bone mineral values are calculated by taking the ratio of the average Q value for all "bone" points for air and the bone-like phantom, in this experiment plaster and aluminum, in each region of interest. The bone mineral density (BMD) is then calculated by multiplying the density of the bone-like phantom to the ratio of the Q value of air over the Q value of the phantom used in the scan

$$BMD = \frac{Q_{air}}{Q_{Phantom}} \times \rho \tag{3}$$

where the ρ is density and the units of BMD are g/cm^2.

G. Converting DXA Results for various manufacturers

There are three different major manufactures of DXA scanners. With different techniques used for each, results and calculations will differ from one another. Thus, Tables VI[1] and VII[1] were formed to provide the correction in achieving similar results between scanners. The tests performed only dealt with Hologic DXA scanner, which make these equations necessary for comparing other DXA scanners results to those results obtained with in a CT scanner.

TABLE VI

CONVERSION FORMULAS FOR BMD IN PROXIMAL FEMUR BETWEEN DXA DEVICES[1]

Hologic QDR-2000 $Neck_{BMD}$ = (0.836 x Lunar DPX-L $Neck_{BMD}$) – 0.008
Hologic QDR-2000 $Neck_{BMD}$ = (0.836 x Norland XR 26 $Neck_{BMD}$) + 0.051
Lunar DPX-L $Neck_{BMD}$ = (1.013 x Hologic QDR-2000 $Neck_{BMD}$) + 0.142
Lunar DPX-L $Neck_{BMD}$ = (0.945 x Norland XR 26 $Neck_{BMD}$) + 0.115
Norland XR 26 $Neck_{BMD}$ = (0.961 x Lunar DPX-L $Neck_{BMD}$) – 0.037
Norland XR 26 $Neck_{BMD}$ = (1.030 x Hologic QDR-2000 $Neck_{BMD}$) + 0.058

TABLE VII

CONVERSION FORMULAS FOR BMD IN THE AP SPINE BETWEEN DXA DEVICES[1]

Hologic QDR-2000 $Spine_{BMD}$ = (0.906 x Lunar DPX-L $Spine_{BMD}$) – 0.025
Hologic QDR-2000 $Spine_{BMD}$ = (0.912 x Norland XR 26 $Spine_{BMD}$) + 0.088
Lunar DPX-L $Spine_{BMD}$ = (1.074 x Hologic QDR-2000 $Spine_{BMD}$) + 0.054
Lunar DPX-L $Spine_{BMD}$ = (0.995 x Norland XR 26 $Spine_{BMD}$) + 0.135
Norland XR 26 $Spine_{BMD}$ = (0.983 x Lunar DPX-L $Spine_{BMD}$) – 0.112
Norland XR 26 $Spine_{BMD}$ = (1.068 x Hologic QDR-2000 $Spine_{BMD}$) – 0.070

V. RESULTS AND DISCUSSION

A. DXA Scans

Figures 22 through 26 show the DXA results from the pig femur specimen #1 and #2. Table VIII shows the vales that are compared to the digital X-ray results from each scan. The *k* values of each scan are also compared.

TABLE VIII

REGIONS USED IN COMPARISON WITH QCT RESULTS FOR PROXIMAL PIG FEMUR SPECIMEN #1

	Region	Est. Area (cm^2)	Est. BMC (g)	BMD (g/cm^2)
Proximal pig femur specimen #1	Neck	7.44	6.60	0.887
	Ward	1.25	1.23	0.981
	Inter	27.87	32.50	1.166
	Total	48.11	52.53	1.092
Proximal pig femur specimen #2 Day 1 of Repeatability	Neck	9.27	11.22	1.210
	Ward	1.05	1.19	1.141
	Inter	41.84	56.60	1.353
	Total	62.98	85.22	1.351
Proximal pig femur specimen #2 Day 2 of Repeatability	Neck	6.72	8.28	1.233
	Ward	1.08	1.29	1.193
	Inter	21.61	29.95	1.386
	Total	50.09	66.26	1.323
Proximal pig femur specimen #2 Day 3 of Repeatability	Neck	6.83	8.27	1.210
	Ward	1.01	1.17	1.165
	Inter	20.33	29.53	1.453
	Total	47.50	62.80	1.322
Distal pig femur specimen #2	Neck	4.85	10.02	2.068
	Ward	1.08	0.89	0.828
	Inter	45.85	60.09	1.311
	Total	79.42	121.12	1.525

Two pig femurs, specimen #1 and #2, were scanned with the DXA to provide a baseline. The DXA results give a known BMD output that is compared to digital X-ray calculations. The DXA scans were repeated four times. Due to the inability to scan the exact area for each trial, the operator could repeat each trial exactly over the course of

time as different specimens were used. Each trial had four different area measurements, the neck, ward, inter and total taken to provide an accurate range to compare with digital X-ray calculations.

For the trials involving the proximal side of the pig femurs, shown in Figures 22 through 25, the BMD results ranged from 1.1 to 1.4 g/cm^2. This proves all the DXA scans are accurate even though the same regions were not scanned consistent each time. The distal side of pig femur specimen #2 shows an increase in BMD. The distal side was known to be denser and thus scanned to provide yet more proof that the DXA scans were accurate.

B. Digital X-ray Scans on the pig femur specimen #1.

A total of six scans were performed using the pig femur specimen #1. Table IX shows the k value results for the 1^{st}, 2^{nd}, and 3^{rd} regions used in the calculations. Figures 27 through 53, found in the Appendix, show each region for each scan with the specific phantom used compared to the calculated Q value from the grayscale value at each pixel that are considered "bone" points with a grayscale areas next to the pictures of the sections scanned. The grayscale areas show where the "bone" points on the sections were located. The "bone" points are highlighted gray in Figures 29, 32, 35, 41, 44, 47, 50, and 53. Tables XVIII through XX show the digital X-ray and DXA BMD calculations and differences for the 1^{st}, 2^{nd}, and 3^{rd} regions of specimen #1 using the plaster phantom.

TABLE IX

THE *k* VALUES FOR EACH REGION USED FOR CALCULATION

Regions	*k* Value
1st	0.320516
2nd	0.250827
3rd	0.309548

TABLE X

DIGITAL X-RAY AND DXA BMD CALCULATIONS AND DIFFERENCES FOR EACH REGION OF SPECIMEN #1 USING THE PLASTER PHANTOM

Region	BMD	Digital X-ray (g/cm^2)	DXA (g/cm^2)	Difference (g/cm^2)	Difference (%)
1st	Area of Interest	1.196	0.887	0.309	25.837
	Overall Highest	-	1.166	0.030	2.510
2nd	Area of Interest	1.342	0.887	0.455	33.916
	Overall Highest	-	1.166	0.176	13.130
3rd	Area of Interest	1.243	0.887	0.356	28.662
	Overall Highest	-	1.166	0.077	6.223

Each *k* value for the regions were considered accurate among the digital X-ray scans. Though, the DXA *k* value of 1.179 is almost two to three times greater the *k* values measured in digital X-ray. The neck region, area of interest, in DXA produced the lowest BMD. The highest BMD in the digital X-ray was comparable to the DXA BMD measurements. Though, all digital X-ray BMD measurements were slightly above the range of DXA BMD measurements. Each day's trial produced results for comparison to the other days in the trial. These results in digital X-ray compared to the DXA results are slightly different though considered accurate.

C. Digital X-ray and DXA Repeatability Test.

The bone femur specimen #2 was scanned on three separate days on effort to measure repeatability. Both digital X-ray and DXA scans were taken each day for comparison. Tables XI through XIII show each day's scans and the difference in the results from both scanners with each phantom.

TABLE XI

DIGITAL X-RAY AND DXA BMD CALCULATIONS AND DIFFERENCES FOR SPECIMEN #2 ON DAY 1 USING BOTH PHANTOMS

Phantom	BMD	Digital X-ray (g/cm^2)	DXA (g/cm^2)	Difference (g/cm^2)	Difference (%)
Plaster	Area of Interest	1.251	1.210	0.041	3.242
	Overall Highest	-	1.456	0.205	16.430
	Overall Lowest	-	1.141	0.110	8.760
Aluminum	Area of Interest	3.424	1.210	2.213	64.658
	Overall Highest	-	1.456	1.968	57.473
	Overall Lowest	-	1.141	2.283	66.673

TABLE XII

DIGITAL X-RAY AND DXA BMD CALCULATIONS AND DIFFERENCES FOR SPECIMEN #2 ON DAY 2 USING BOTH PHANTOMS

Phantom	BMD	Digital X-ray (g/cm^2)	DXA (g/cm^2)	Difference (g/cm^2)	Difference (%)
Plaster	Area of Interest	1.371	1.233	0.138	10.088
	Overall Highest	-	1.386	0.015	1.069
	Overall Lowest	-	1.193	0.178	13.005
Aluminum	Area of Interest	3.367	1.233	2.134	63.377
	Overall Highest	-	1.386	1.981	58.833
	Overall Lowest	-	1.193	2.173	64.565

TABLE XIII

DIGITAL X-RAY AND DXA BMD CALCULATIONS AND DIFFERENCES FOR SPECIMEN #2 ON DAY 3 USING BOTH PHANTOMS

Phantom	BMD	Digital X-ray (g/cm^2)	DXA (g/cm^2)	Difference (g/cm^2)	Difference (%)
Plaster	Area of Interest	1.193	1.210	0.017	1.384
	Overall Highest	-	1.453	0.259	21.745
	Overall Lowest	-	1.165	0.028	2.386
Aluminum	Area of Interest	2.690	1.210	1.480	55.013
	Overall Highest	-	1.453	1.237	45.978
	Overall Lowest	-	1.165	1.525	56.686

From Tables XI through XIII, the plaster phantom proves to be accurate over the aluminum phantom when comparing the digital X-ray to the DXA results. For the scans

using plaster phantom, the digital X-ray BMD results are relatively close to the DXA results and all fall into the range between the highest and lowest values of BMD that the DXA scanner measures. Tables XIV and XV show the difference between each day for the digital X-ray results using the both phantoms and the DXA results.

TABLE XIV

THE BMD DIFFERENCE BETWEEN EACH DAY FOR THE DIGITAL X-RAY RESULTS USING BOTH PHANTOMS

	Plaster Difference (g/cm^2)	Plaster Difference (%)	Aluminum Difference (g/cm^2)	Aluminum Difference (%)
Day 1 to Day 2	0.108	8.599	0.022	0.959
Day 1 to Day 3	0.061	5.105	0.396	14.721
Day 2 to Day 3	0.169	14.142	0.418	15.539

TABLE XV

THE AREA OF INTEREST, HI, AND LOW BMD DIFFERENCE BETWEEN EACH DAY FOR THE DXA RESULTS

BMD	Day Comparison	Difference (g/cm^2)	Difference (%)
Area of Interest	Day 1 to Day 2	0.023	1.901
	Day 1 to Day 3	0.000	0.000
	Day 2 to Day 3	0.023	1.901
Hi	Day 1 to Day 2	1.456	4.808
	Day 1 to Day 3	1.386	0.206
	Day 2 to Day 3	1.453	4.611
Low	Day 1 to Day 2	0.052	4.557
	Day 1 to Day 3	0.024	2.060
	Day 2 to Day 3	0.028	2.403

Tables XIV through XV show that these experimentations can be repeatable. The difference between the digital X-ray BMD results can be traced to the different regions taken since it was impossible to get the exact region rescanned due to repositioning of the specimen in the scanner after each trial. The DXA results are similar for the area of interest, the highest BMD and the lowest BMD measurements.

The digital X-ray BMD results using the plaster phantom are similar to the DXA results as the BMD results using the aluminum phantom are not as similar. The BMD results using the aluminum phantom prove to be almost three times as much as the BMD results using the plaster phantom. The large margin of BMD difference between the phantoms is traced back to the fact the aluminum phantom is almost three times as dense as the plaster phantom. When the aluminum phantom density is multiplied by the bone mineral content over the area ratio, found in Equation 3, the large difference in the BMD results occur. The bone mineral content over the area ratio produces results around 1.0. So when the density is multiplied to this ratio, the BMD results mimic the value of the density used. This is the reason the phantom used in the DXA scanner is "bone-like" material with a similar density to bone.

D. Digital X-ray results with specimen #2 cut in half.

Table XVI shows the digital X-ray BMD results with each phantom for specimen #2 cut in half and the differences between the digital X-ray BMD calculations using a half specimen and DXA BMD calculations using a whole specimen. Tables XVII shows the digital X-ray BMD differences between a whole and half pig femur specimen #2 using both the aluminum and plaster phantoms for each day.

TABLE XVI

DIGITAL X-RAY BMD CALCULATIONS WITH WHOLE SPECIMEN DXA BMD CALCULATIONS AND DIFFERENCES FOR SPECIMEN #2 CUT IN HALF USING BOTH PHANTOMS

Phantom	BMD	Digital X-ray (g/cm^2)	DXA (g/cm^2)	Difference (g/cm^2)	Difference (%)
Plaster	Area of Interest	1.045	1.210	0.165	15.787
	Hi	-	1.453	0.408	39.040
	Low	-	1.165	0.120	11.481
Aluminum	Area of Interest	2.511	1.210	1.301	51.807
	Hi	-	1.453	1.058	42.128
	Low	-	1.165	1.346	53.599

TABLE XVII

DIGITAL X-RAY BMD CALCULATIONS AND DIFFERENCES BETWEEN A WHOLE AND HALF PIG FEMUR SPECIMEN #2 USING BOTH PHANTOMS ON EACH DAY

Day	Phantom	Digital X-ray of Half Femur (g/cm^2)	Digital X-ray of Whole Femur (g/cm^2)	Difference (g/cm^2)	Difference (%)
1	Plaster	1.045	1.251	0.206	16.467
	Aluminum	2.511	3.424	0.913	26.647
2	Plaster	1.045	1.371	0.326	23.778
	Aluminum	2.511	3.367	0.856	25.423
3	Plaster	1.045	1.193	0.148	12.406
	Aluminum	2.511	2.690	0.179	6.654

Table XVI shows that the digital X-ray BMD measurement using the plaster phantom was slightly lower then the measurement recorded in Table XIII of 1.193 g/cm^2. Though slightly lower, the digital X-ray BMD measurement still remains in the range of the DXA BMD measurements. The digital X-ray BMD measurement using the

aluminum phantom, shown in Table XVI, also proved to be slightly lower then the measurement recorded in Table XIII of 2.690 g/cm^2. The results from Tables XVI and XVII compared to DXA BMD measurements show accuracy.

The digital X-ray BMD measurements of pig femur specimen #2 cut in half did not meet the expectations of achieving the same result as a whole pig femur specimen #2, even though the results for the femur cut in half were only slightly lower. Table XVII shows that day 1 and 2 have significant difference with the use of the plaster or aluminum phantom. Day 3 shows more of a similarity between the digital X-ray BMD of the half and whole femur, yet neither results for the half specimen fell within the range of BMD provided by the DXA scans. The repeatability tests proved to fall within the BMD range measured by the DXA for the whole bone, but the trial with the half femur did not. This proves that there is inaccuracy in the BMD calculations and the experimentation with the phantoms.

E. Digital X-ray and DXA calculations from the distal end of specimen #2.

Tables XXXIX and XXXX show the digital X-ray BMD calculations with whole specimen DXA BMD calculations and the differences in the distal end for specimen #2 using the plaster and aluminum phantoms.

TABLE XVIII

DIGITAL X-RAY BMD CALCULATIONS WITH WHOLE SPECIMEN DXA BMD CALCULATIONS AND DIFFERENCES OF THE DISTAL END FOR SPECIMEN #2 USING BOTH PHANTOMS

Phantom	BMD	Digital X-ray (g/cm^2)	DXA (g/cm^2)	Difference (g/cm^2)	Difference (%)
Plaster	Area of Interest	1.219	1.775	0.556	45.618
	Hi	-	2.068	0.849	69.655
	Low	-	0.828	0.391	32.073
Aluminum	Area of Interest	3.024	1.775	1.249	41.309
	Hi	-	2.068	0.956	31.621
	Low	-	0.828	2.196	72.622

Table XVIII shows that once again the digital X-ray BMD measurement with the plaster phantom is within the DXA BMD measurement range and the digital X-ray BMD measurement with the aluminum phantom is not. The digital X-ray BMD measurements in Table XVIII have a larger difference in BMD between the digital X-ray and DXA results shown in Table XVII. Also, the digital X-ray BMD measurements are very similar to Table XVI. It is observed in all experimentations that these digital X-ray BMD measurements reflect a similar BMD to the phantom used. This means that the Q air value over the Q phantom value ratio is approximately one.

This experiment, as well as the experiment with the half femur, shows an inaccuracy in the BMD calculations. It was known that the distal side of the femur was thicker then the proximal side by a significant amount. Table XVIII shows the BMD calculation for the distal side of 1.219 g/cm^2 was actually less compared to day 1 and 2

measurements of pig femur specimen #2. Day 1 and 2 measurements of the pig femur specimen #2 were 1.251 and 1.371 g/cm^2 with the plaster phantom, respectively. Table XVIII also shows the distal side of 3.024 g/cm^2 is less compared to day 1 and 2 measurements of pig femur specimen #2 of 3.424 and 3.367 g/cm^2 with the aluminum phantom, respectively.

F. DXA Scan Manufacturer Conversions.

Table XIX shows the calculations from the formulas used in Table VI and VII for the neck section of a femur bone. As an example, Table XIX shows the difference in measurements that different manufacturers produce. The 3rd section measured is defined as the neck section from the DXA results. In order to compare the digital X-ray BMD calculations to any engineering literature published with DXA measurements, the equations from Tables VI and VII are needed for conversion. The digital X-ray BMD equations developed in this experiment are only based on a Hologic DXA scanner and it has been proven by the publishing "Bone Densitometry in Clinical Practice" that calculation differences do exist between the major DXA manufacturers.[1]

TABLE XIX

THE BMD, DIFFERENCE AND % DIFFERENCE FOR EACH DXA MANUFACTURER COMPARED TO HOLOGIC DXA RESULTS AND CALCULATED DXA RESULTS FROM A DIGITAL X-RAY SCANNER USING FORMUALS FROM TABLE VI &VII

	Hologic	Lunar	Norland
BMD	1.243	1.205	1.138
Difference from DXA	-	0.156	0.089
% Difference from DXA	-	12.92	7.86
Difference from Digital X-ray	0.194	0.039	0.105
% Difference from Digital X-ray	15.63	2.94	8.28

VI. CONCLUSIONS

A. DXA Scans

The BMD results of the DXA scans were similar to those obtained by previous studies of femurs. The distal femur had greater BMD values than the proximal end. The BMD results from the repeatability study were consistent despite variation in the selected areas.

B. Digital X-ray Scans on the pig femur specimen #1.

The three bone regions evaluated with the digital X-ray were different than the regions scanned with the DXA because the DXA regions are predefined by the software. All results from each region in the digital X-ray were larger than the highest BMD attained in the DXA. The k values, from the digital X-ray, were two to three times lower than the k values from the DXA scans. The Q-value histograms developed in Microsoft Excel from the grayscale data showed the same pattern and peaks typically obtained from the DXA.

C. Digital X-ray and DXA Repeatability Test.

The tests were repeatable for both the plaster and aluminum phantoms. The proposed theory that any material can be used as a phantom for BMD calculations was unattainable. The digital X-ray BMD results using the plaster phantom were similar to the DXA results, while the aluminum phantom BMD results were much higher than the DXA results.

D. Digital X-ray results with specimen #2 cut in half.

The results showed that the BMD results for the half bone specimens were slightly lower than the whole bone specimens.

E. Digital X-ray and DXA calculations from the distal end of specimen #2.

The BMD for the distal end of the pig femur specimen was higher than the proximal end for the DXA scanner but similar when using the digital X-ray system. Since the distal end is thicker, the BMD should be greater. The equations used to calculate the BMD from the digital X-ray system are in error.

F. DXA Scan Manufacturer Conversions.

The conversion equations can be used to compare results from different DXA scanners.

VII. RECOMMENDATIONS

If the DXA software is capable of selecting arbitrary areas, then composite bones and smaller specimens could be measured. To verify the DXA results for the pig distal femur, repetitive tests should be performed.

If the Hologic system is used, a better understanding of the factors involved in calculating the BMD is necessary. Although Hologic was unwilling to disclose details of the calculations, it may be helpful to review the two Hologic articles and contact them with specific questions. Since the histograms for both the DXA and digital X-ray system are similar, the digital X-ray BMD calculation is in error and should be investigated.

The plaster phantom should be used with the digital X-ray system until the BMD calculation errors can be resolved. Once these issues are resolved, testing with other phantoms could be explored.

VIII. REFERENCES

1. Bonnick, S.L., “Bone Densitometry in Clinical Practice,” Humana Press Inc. 1998; Texas, USA

2. Blake, G., Wahner, H., Fogelman, I., “The Evaluation of Osteoporosis: Dual Energy X-ray Absorptiometry and Ultrasound in Clinical Practice,” Martin Dunitz Ltd 1999; United Kindgom

3. Lee, Joseph K.T., Sagel, Stuart S., Stanely, Robert J., “Computed Body Tomography,” Raven Press 1983; New York, New York

4. Stein, Jay A., Lazewatsky, Joel L., Hochberg, Alan M., “A dual-energy X-ray bone densitomter incorporating an internal reference system,” Hologic Inc. 1987; Waltham, Massachusetts

5. Hologic Inc., Waltham, Massachusetts

6. Norton Health Care Pavilion, Louisville, Kentucky.

IX. APPENDIX

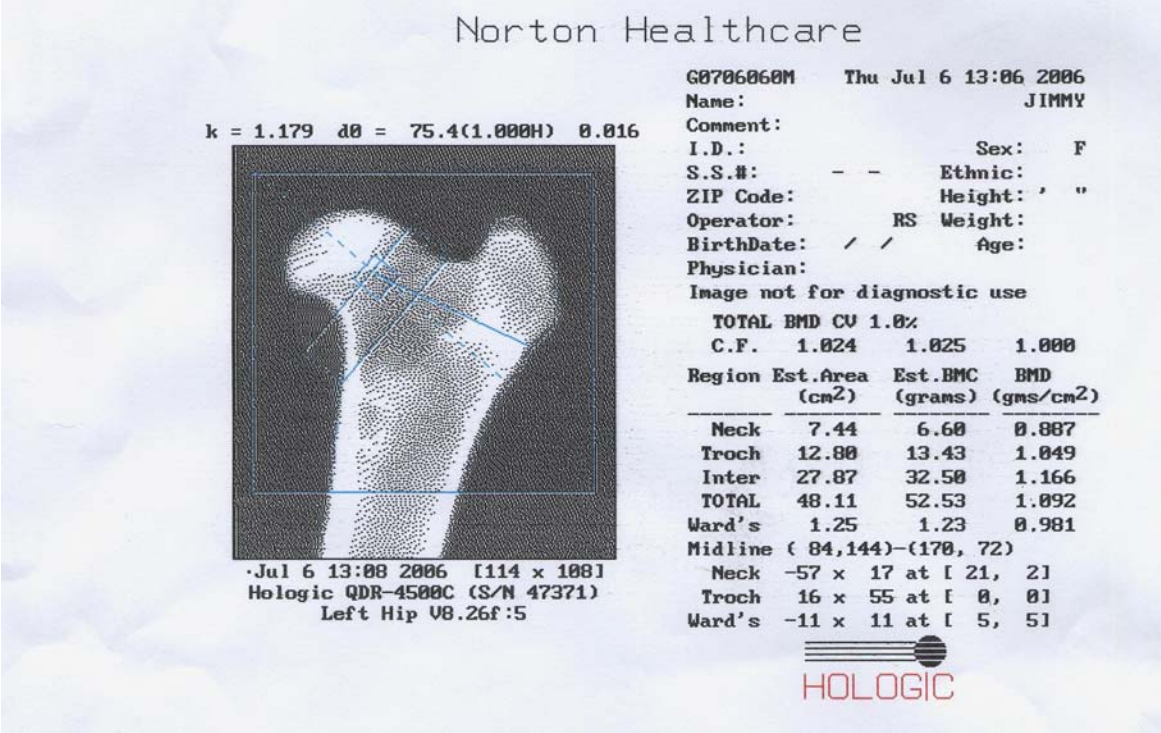

Figure 22. DXA results from pig femur specimen #1.[6]

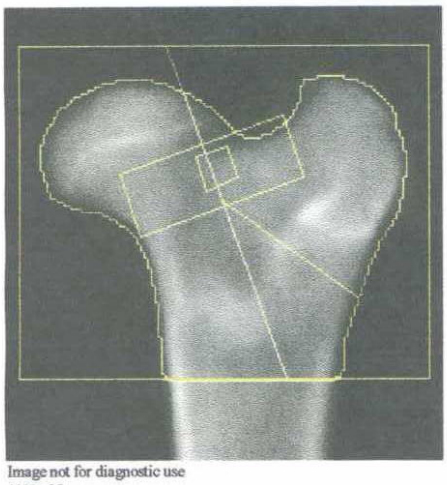

Scan Information:

Scan Date: September 06, 2006 ID: G0906060D
Scan Type: f Left Hip
Analysis: September 06, 2006 13:11 Version 11.2
Left Hip
Operator:
Model: QDR 4500C (S/N 47371)
Comment:

DXA Results Summary:

Region	Area (cm²)	BMC (g)	BMD (g/cm²)	T-Score	Z-Score
Neck	9.27	11.22	1.210	3.2	
Troch	11.88	17.29	1.456	7.5	
Inter	41.84	56.60	1.353	1.6	
Total	**62.98**	**85.11**	**1.351**	**3.4**	
Ward's	1.05	1.19	1.141	3.5	

Figure 23. DXA results from pig femur specimen #2 on day 1.[6]

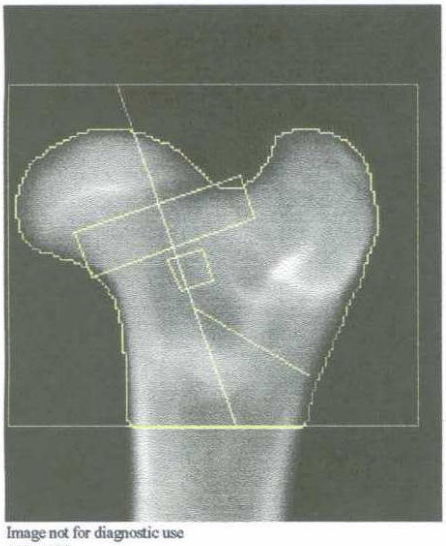

Scan Information:

Scan Date: September 19, 2006 ID: G09190605
Scan Type: f Left Hip
Analysis: September 19, 2006 10:05 Version 11.2
Left Hip
Operator:
Model: QDR 4500C (S/N 47371)
Comment:

DXA Results Summary:

Region	Area (cm^2)	BMC (g)	BMD (g/cm^2)	T - Score	Z - Score
Neck	6.72	8.28	1.233	3.5	
Troch	21.76	28.03	1.288	5.8	
Inter	21.61	29.95	1.386	1.8	
Total	**50.09**	**66.26**	**1.323**	**3.1**	
Ward's	1.08	1.29	1.193	3.9	

Figure 24. DXA results from pig femur specimen #2 on day 2.[6]

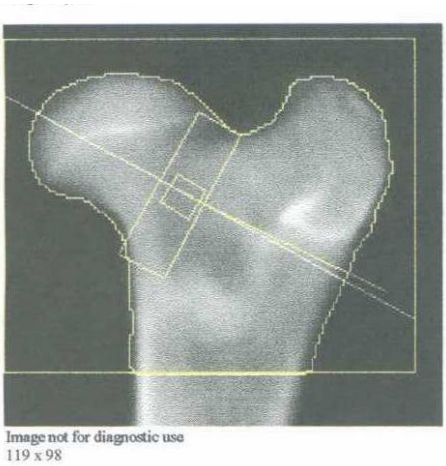

Scan Information:

Scan Date: September 20, 2006 ID: G09200608
Scan Type: f Left Hip
Analysis: September 20, 2006 11:12 Version 11.2
Left Hip
Operator:
Model: QDR 4500C (S/N 47371)
Comment:

DXA Results Summary:

Region	Area (cm^2)	BMC (g)	BMD (g/cm^2)	T - Score	Z - Score
Neck	6.83	8.27	1.210	3.3	
Troch	20.34	25.00	1.229	5.2	
Inter	20.33	29.53	1.453	2.3	
Total	**47.50**	**62.80**	**1.322**	**3.1**	
Ward's	1.01	1.17	1.165	3.7	

Figure 25. DXA results from pig femur specimen #2 on day 3.[6]

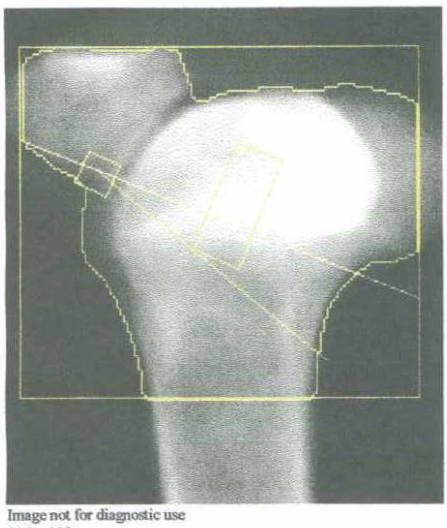

Image not for diagnostic use
116 x 103

Scan Information:

Scan Date: September 06, 2006 ID: G0906060E
Scan Type: f Left Hip
Analysis: September 06, 2006 13:19 Version 11.2
Left Hip
Operator:
Model: QDR 4500C (S/N 47371)
Comment:

DXA Results Summary:

Region	Area (cm^2)	BMC (g)	BMD (g/cm^2)	T - Score	Z - Score
Neck	4.85	10.02	2.068	11.0	
Troch	28.73	51.00	1.775	10.6	
Inter	45.85	60.09	1.311	1.4	
Total	**79.42**	**121.12**	**1.525**	**4.8**	
Ward's	1.08	0.89	0.828	0.8	

Figure 26. DXA results from distal end of the pig femur specimen #2.[6]

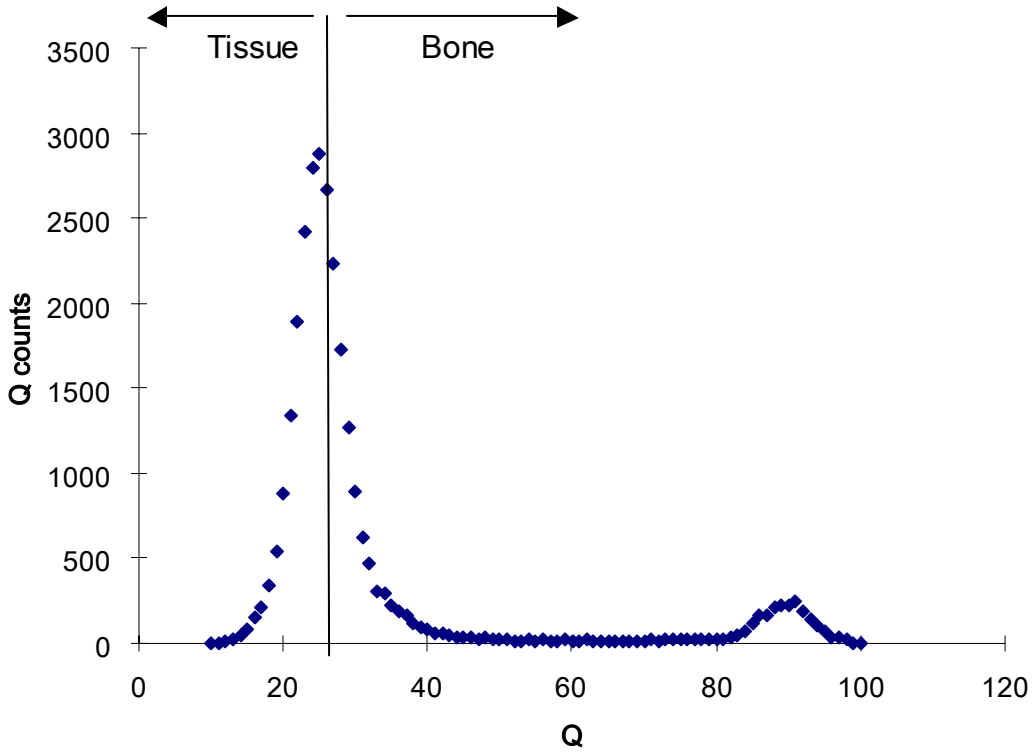

Figure 27. Histogram of the 1st region air scan for the pig femur specimen #1.

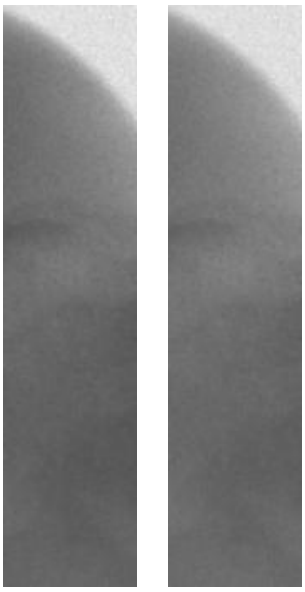

Figure 28. 1st region air scans.

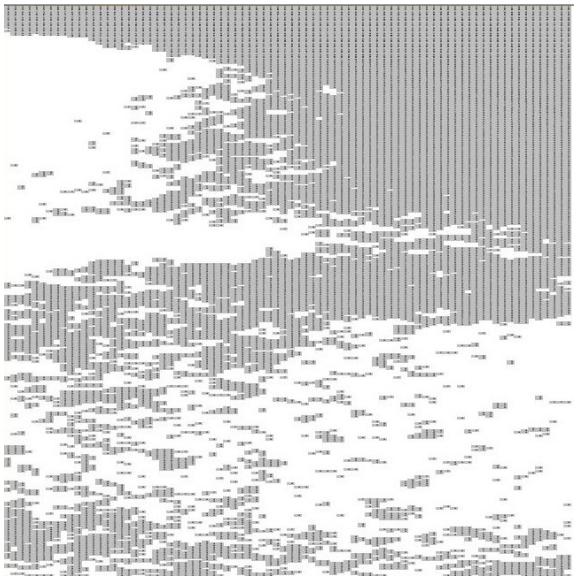

Figure 29. The "bone" points for air.

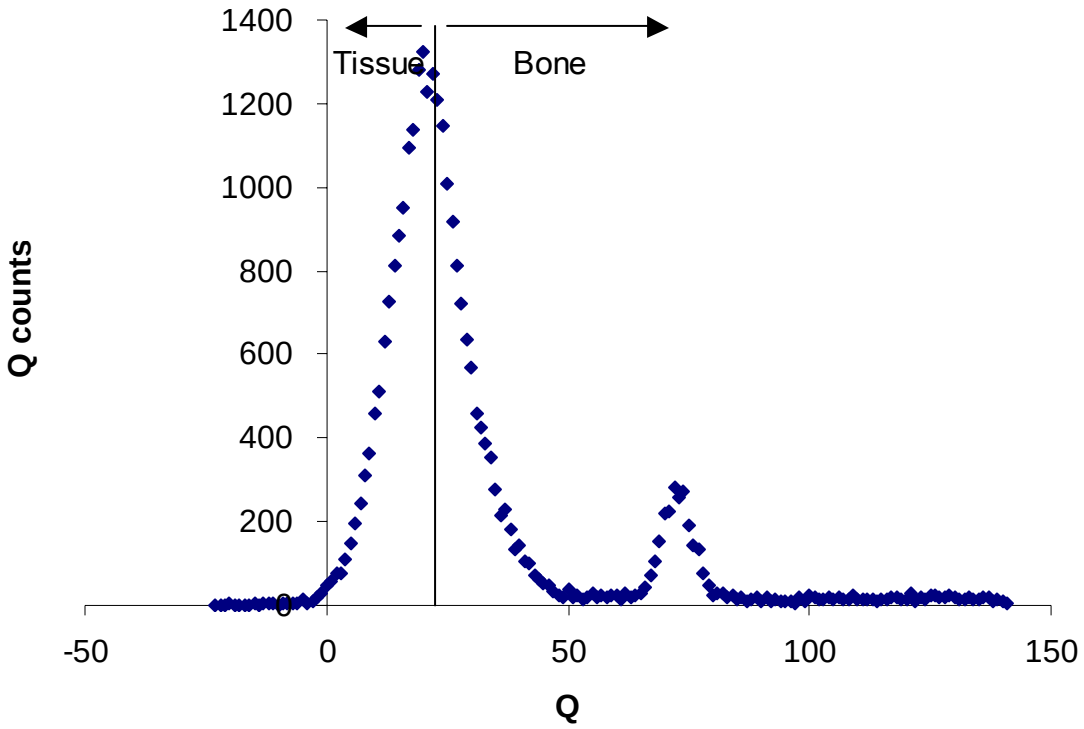

Figure 30. Histogram of the 1st region plaster scan for the pig femur specimen #1.

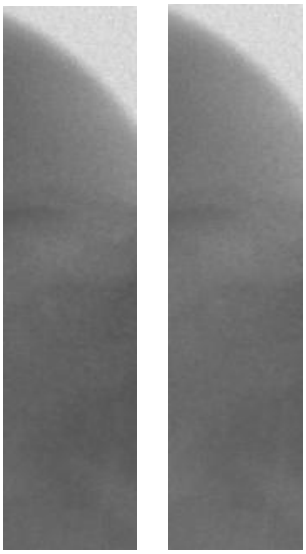

Figure 31. 1st region plaster scans.

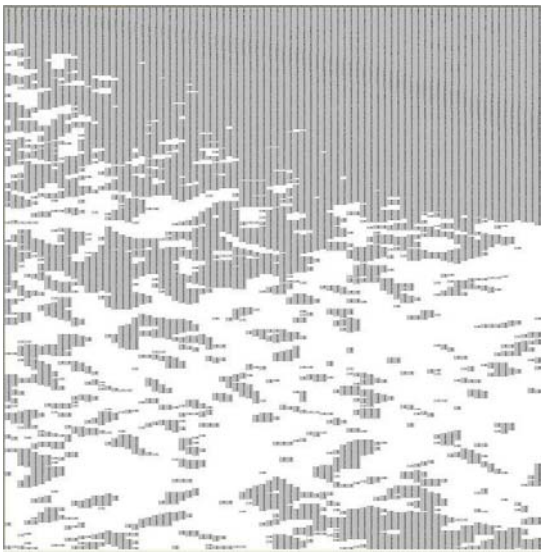

Figure 32. The "bone" points for plaster.

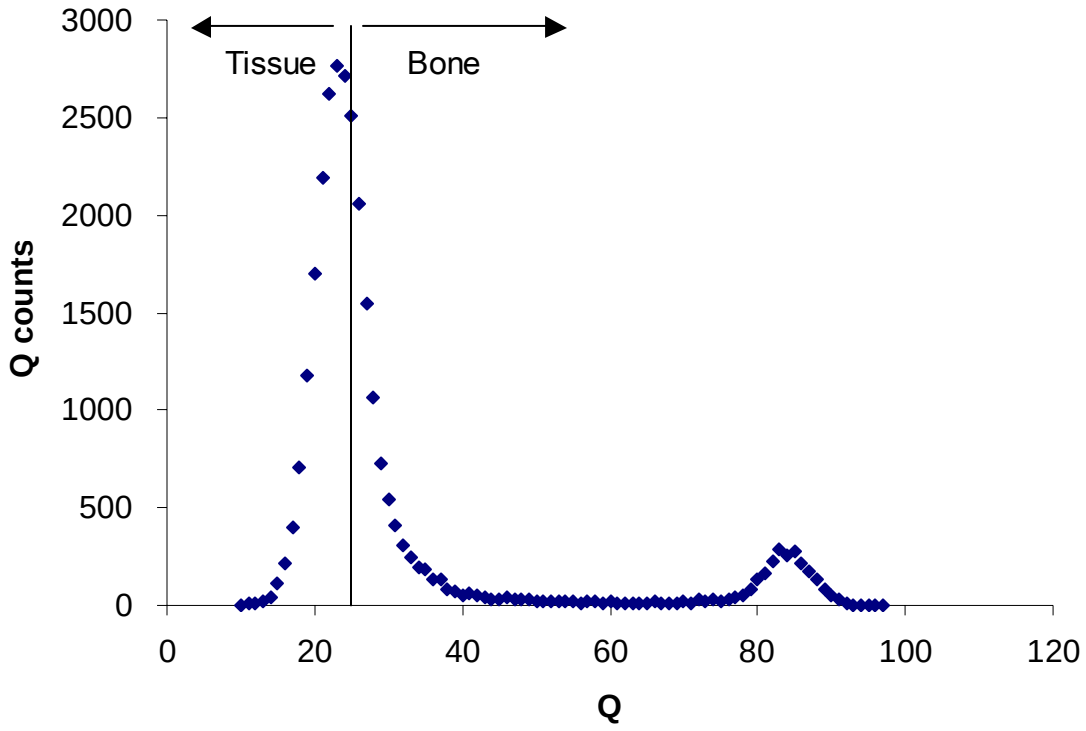

Figure 33. Histogram of the 1st region plexiglass scan for the pig femur specimen #1.

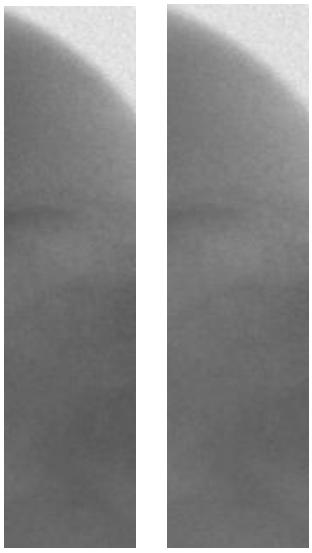

Figure 34. 1st region plexiglass scans.

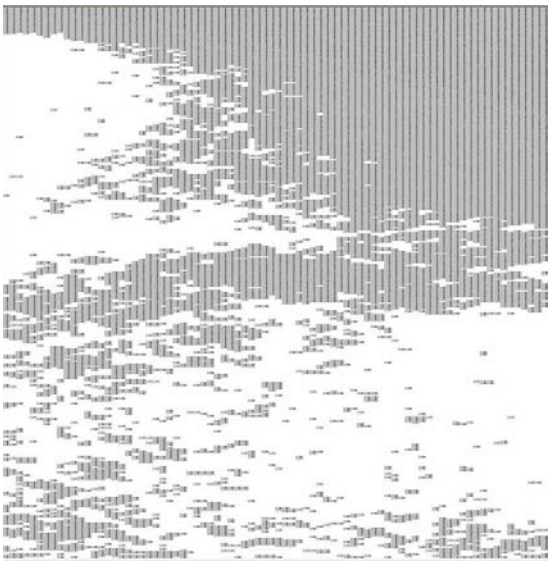

Figure 35. The "bone" points for plexiglass.

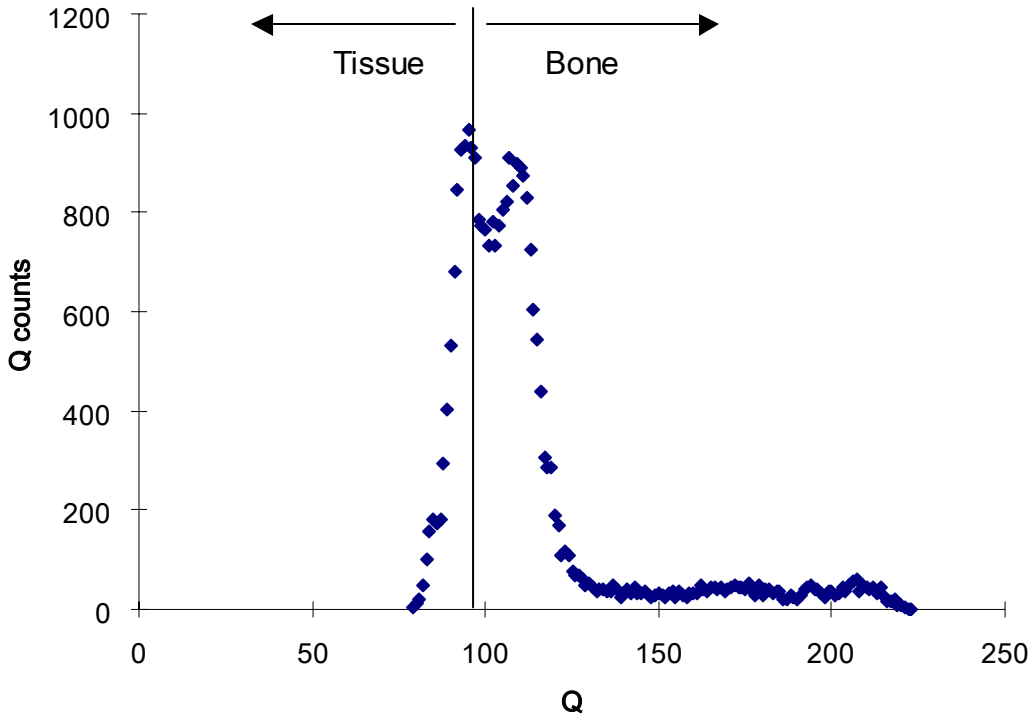

Figure 36. Histogram of the 2nd region air scan for the pig femur specimen #1.

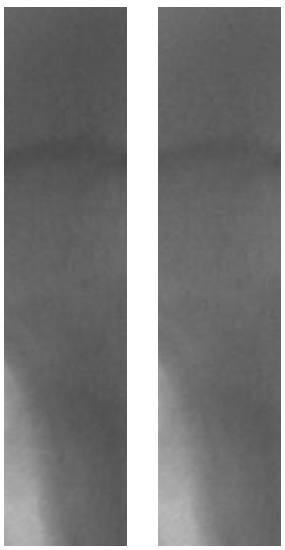

Figure 37. 2nd region air scans.

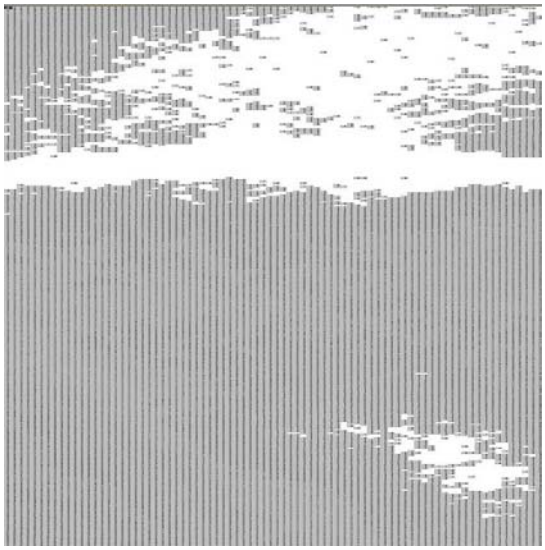

Figure 38. The "bone" points for air.

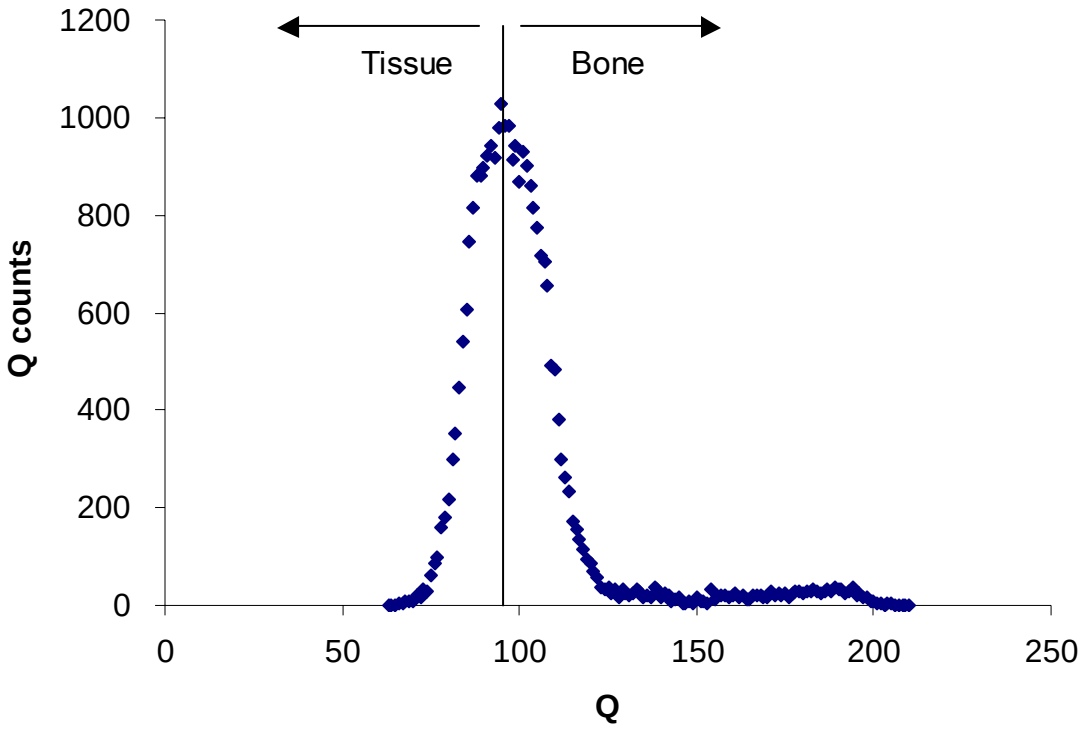

Figure 39. Histogram of the 2nd region plaster scan for the pig femur specimen #1.

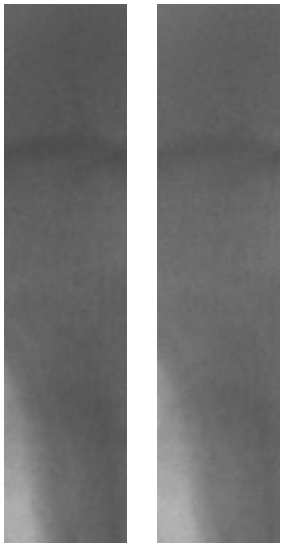

Figure 40. 2nd region plaster scans.

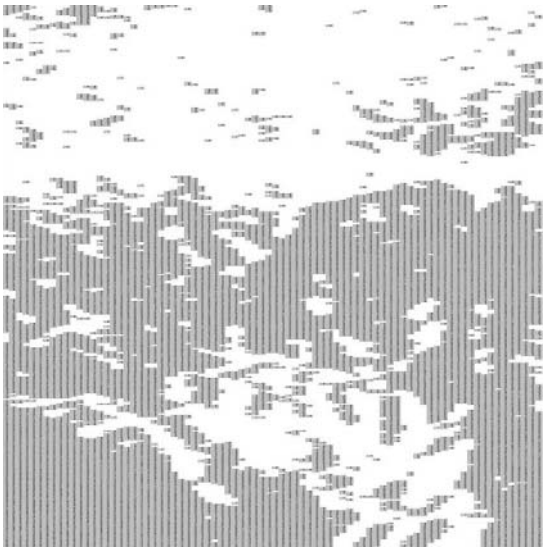

Figure 41. The "bone" points for plaster.

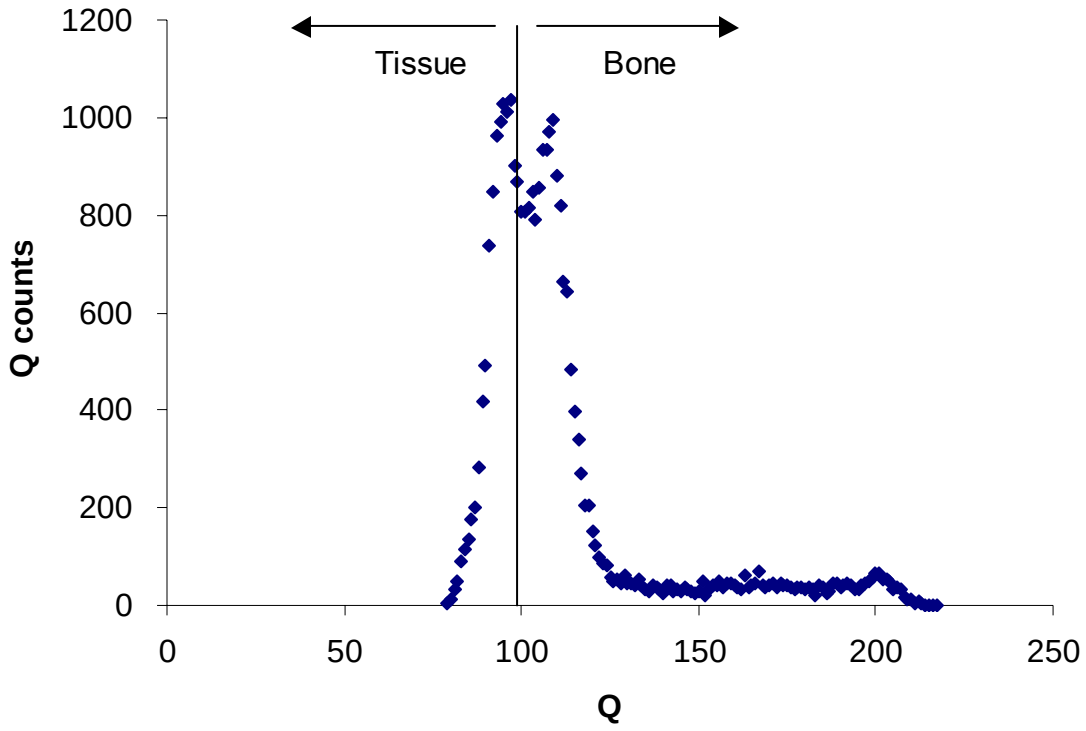

Figure 42. Histogram of the 2nd region plexiglass scan for the pig femur specimen #1.

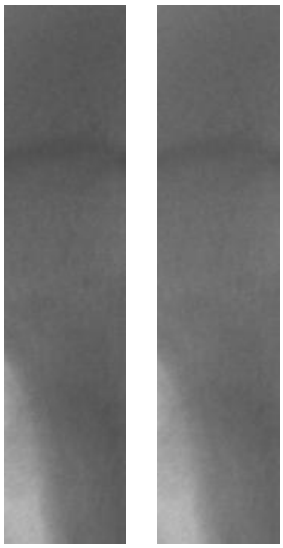

Figure 43. 2nd region plexiglass scans.

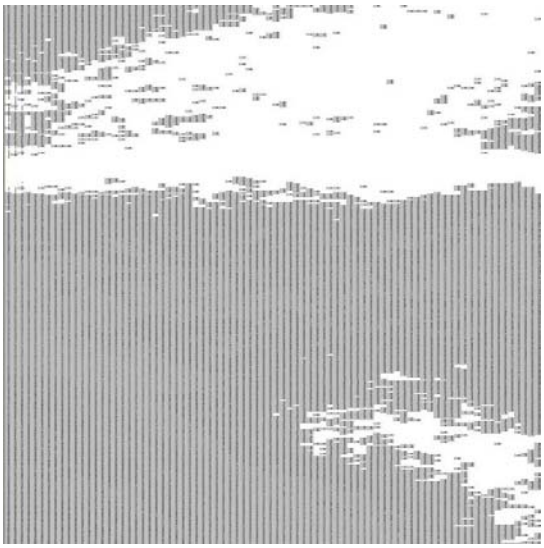

Figure 44. The "bone" points for plexiglass.

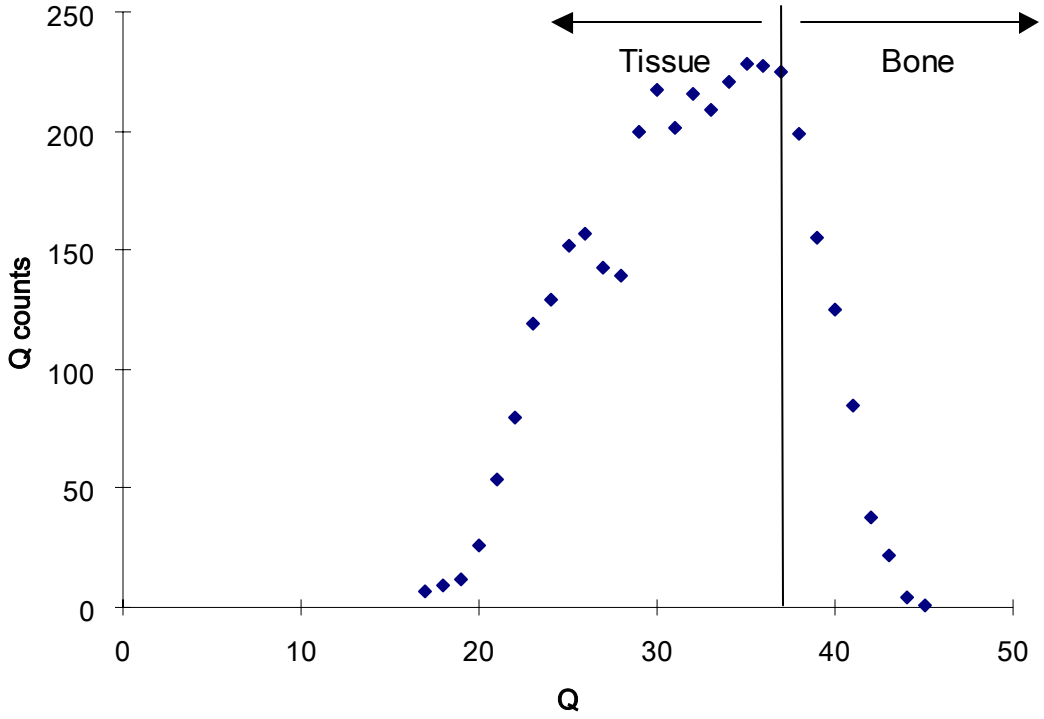

Figure 45. Histogram of the 3rd region air scan for the pig femur specimen #1.

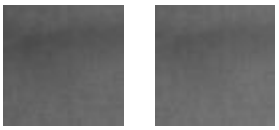

Figure 46. 3rd region air scans.

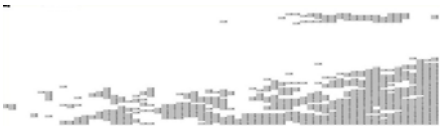

Figure 47. The "bone" points for air.

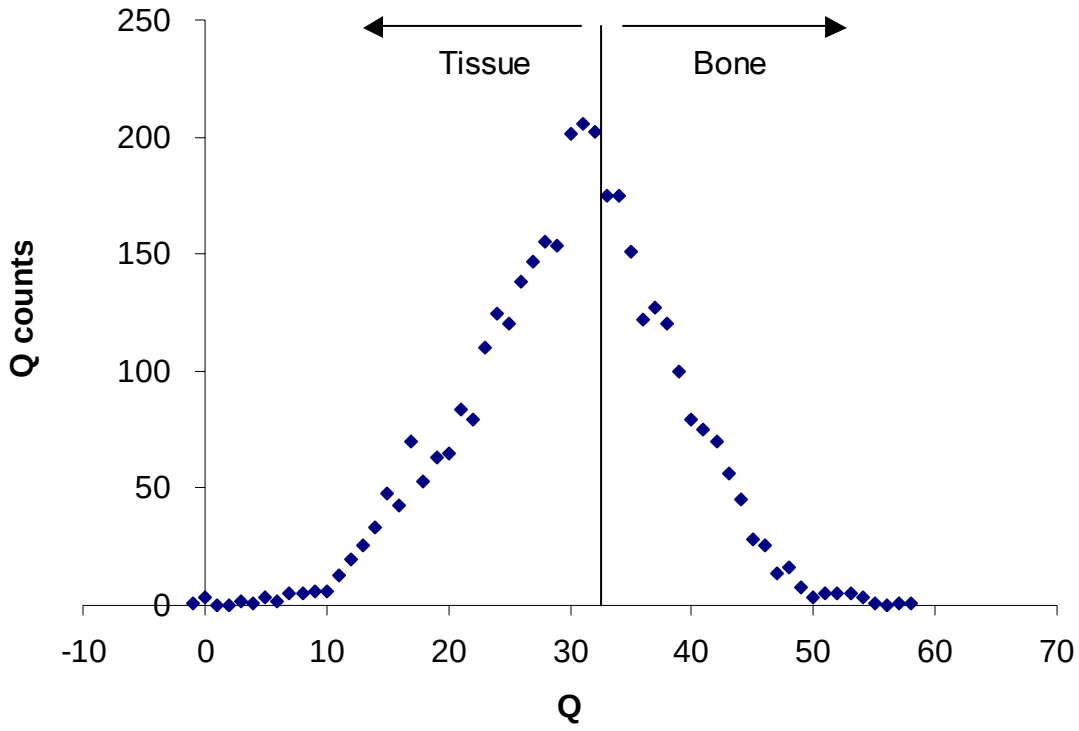

Figure 48. Histogram of the 3rd region plaster scan for the pig femur specimen #1.

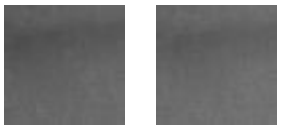

Figure 49. 3rd region plaster scans.

Figure 50. The "bone" points for plaster.

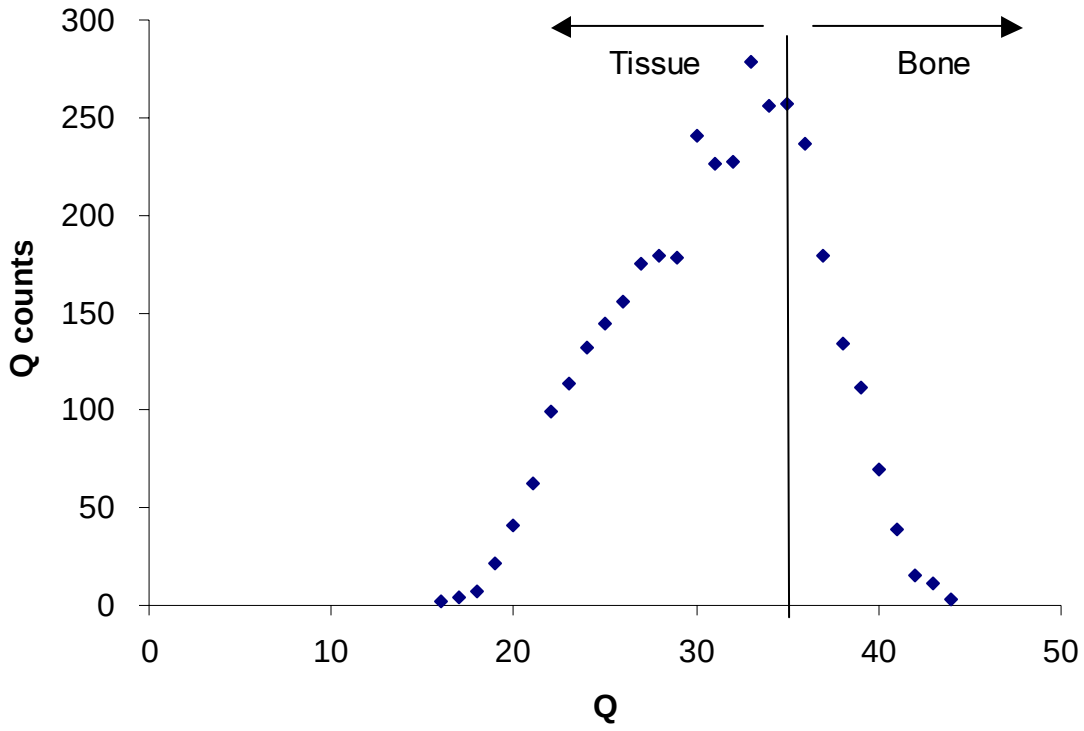

Figure 51. Histogram of the 3rd region plexiglass scan for the pig femur specimen #1.

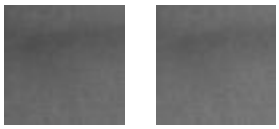

Figure 52. 3rd region plexiglass scans.

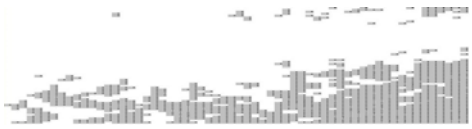

Figure 53. The "bone" points for plexiglass.

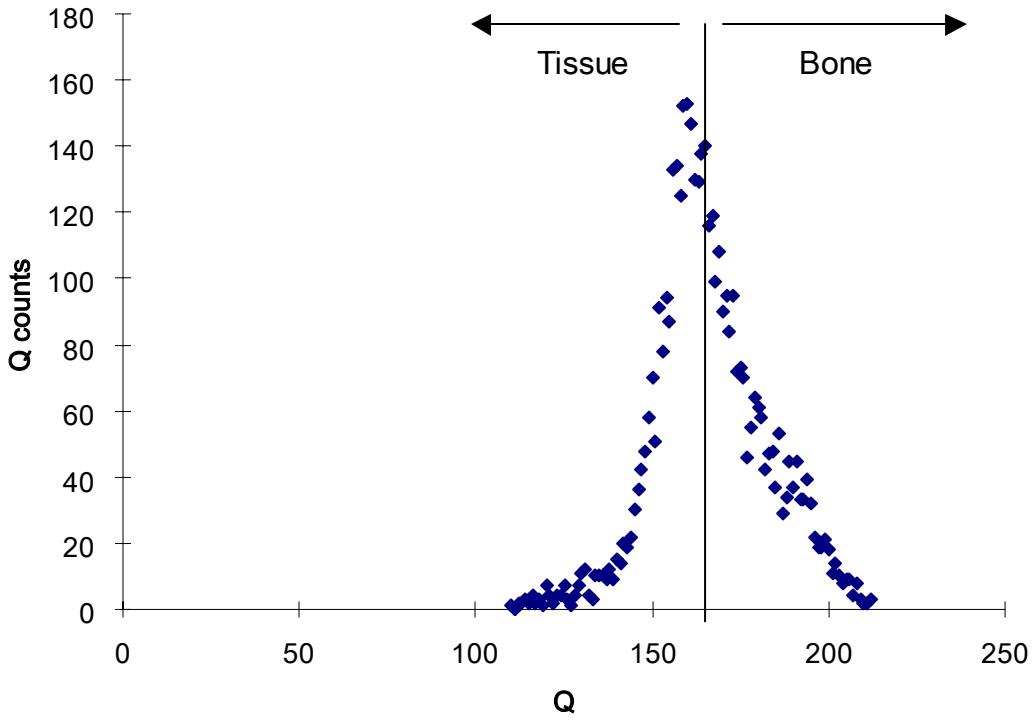

Figure 54. Histogram of the 1st day region air scan for the pig femur specimen #2.

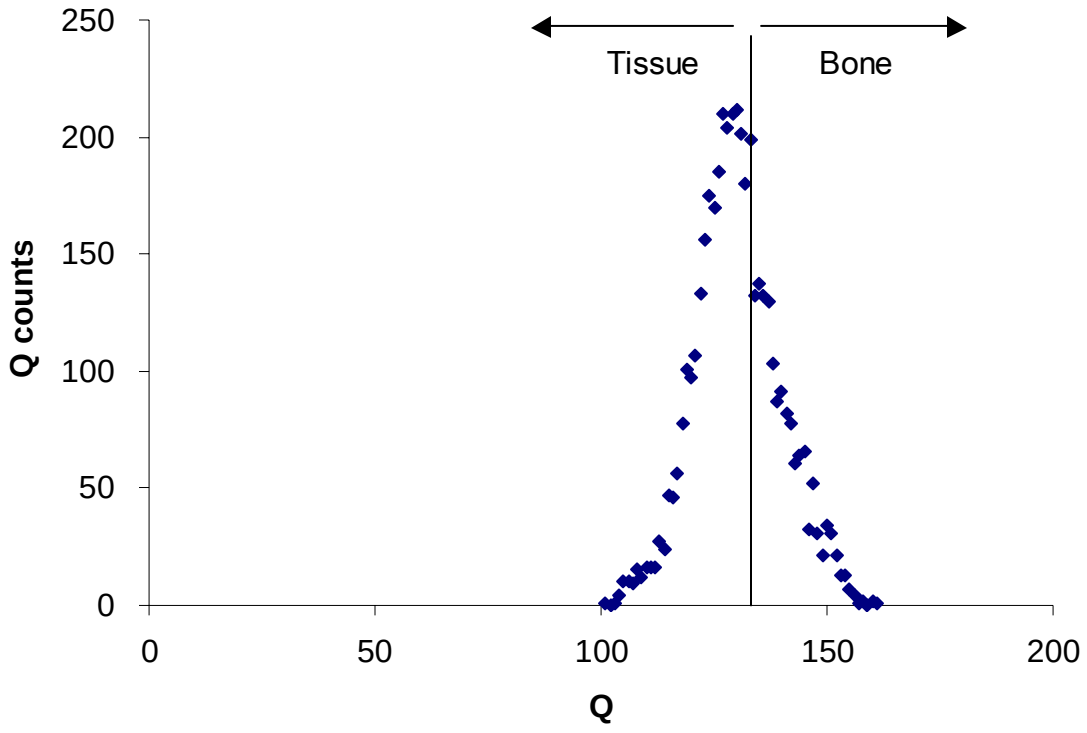

Figure 55. Histogram of the 1st day region aluminum scan for the pig femur specimen #2.

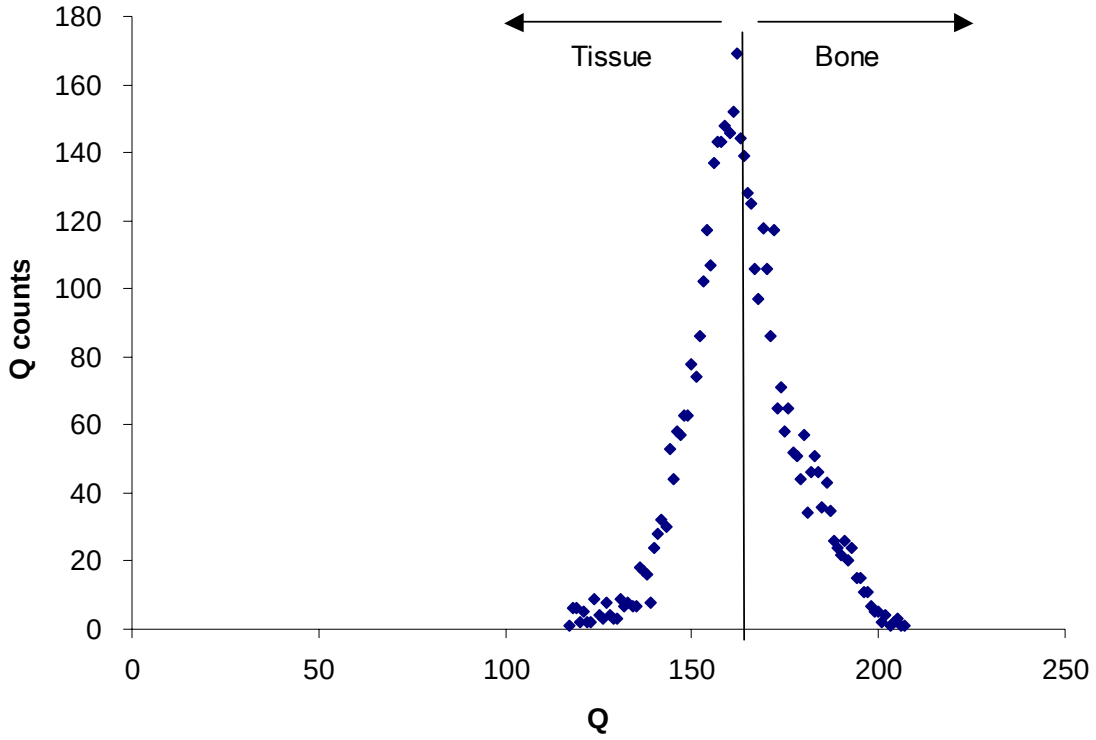

Figure 56. Histogram of the 1st day region plexiglass scan for the pig femur specimen #2.

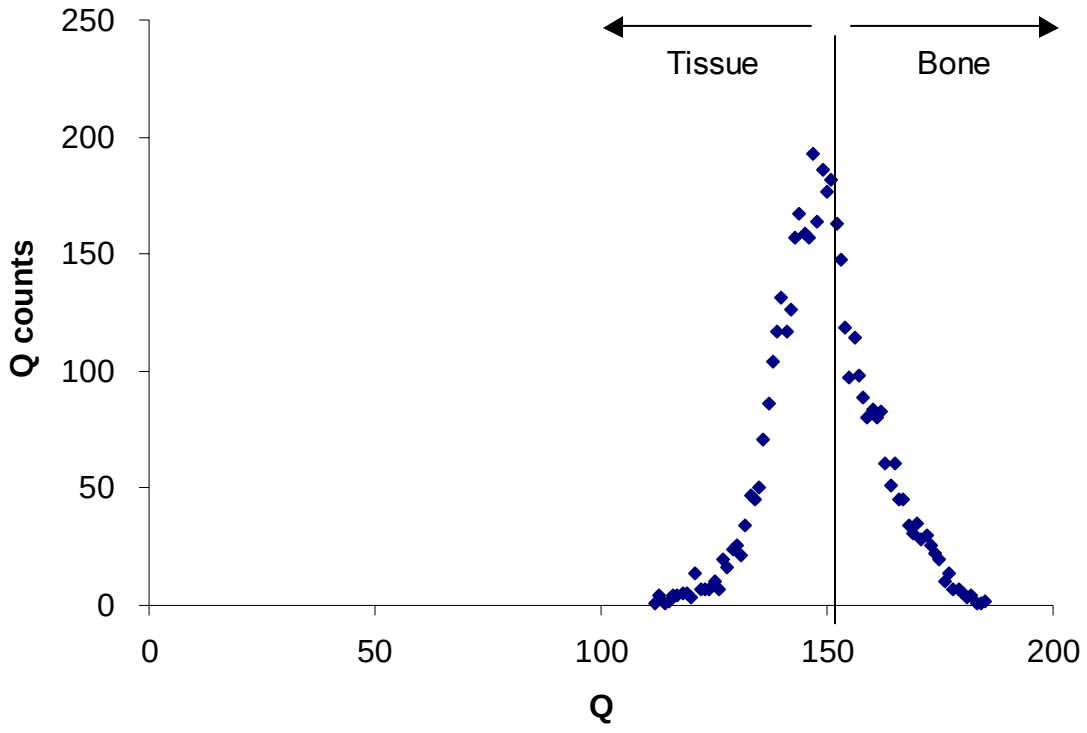

Figure 57. Histogram of the 1st day region plaster scan for the pig femur specimen #2.

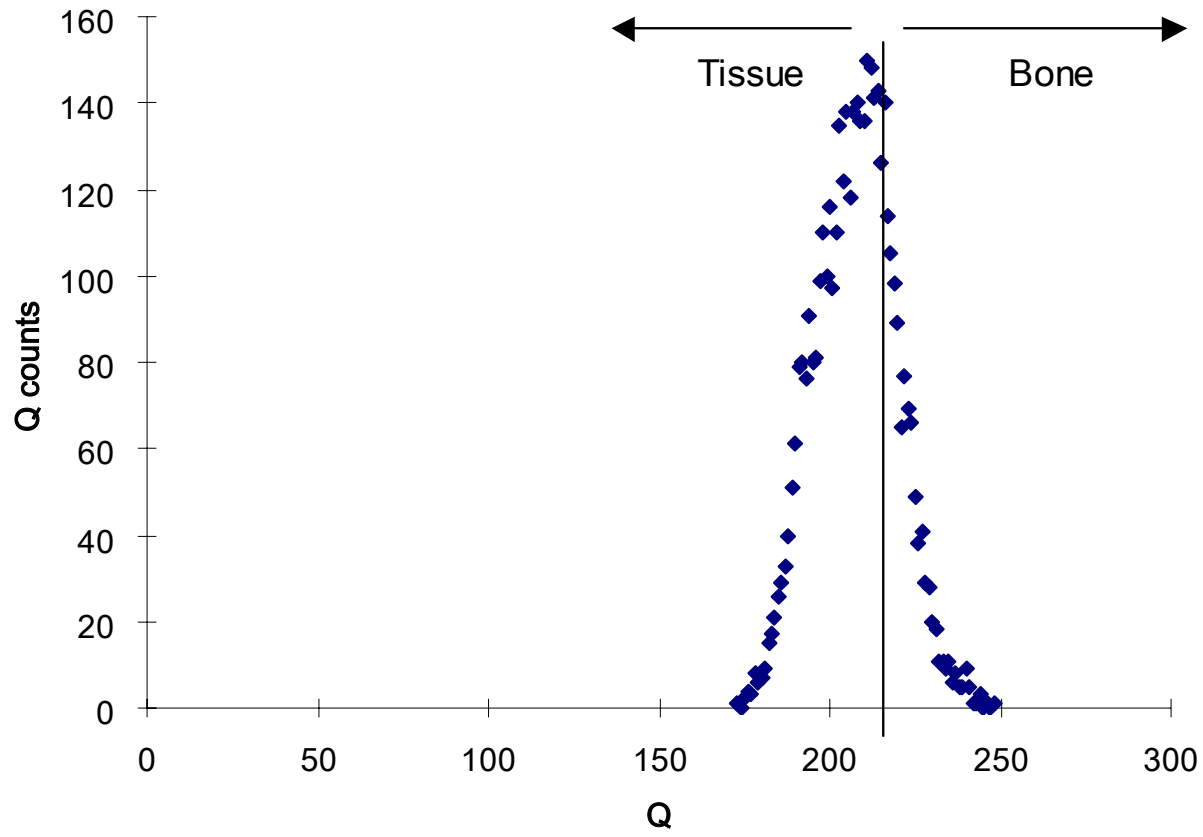

Figure 58. Histogram of the 2nd day region air scan for the pig femur specimen #2.

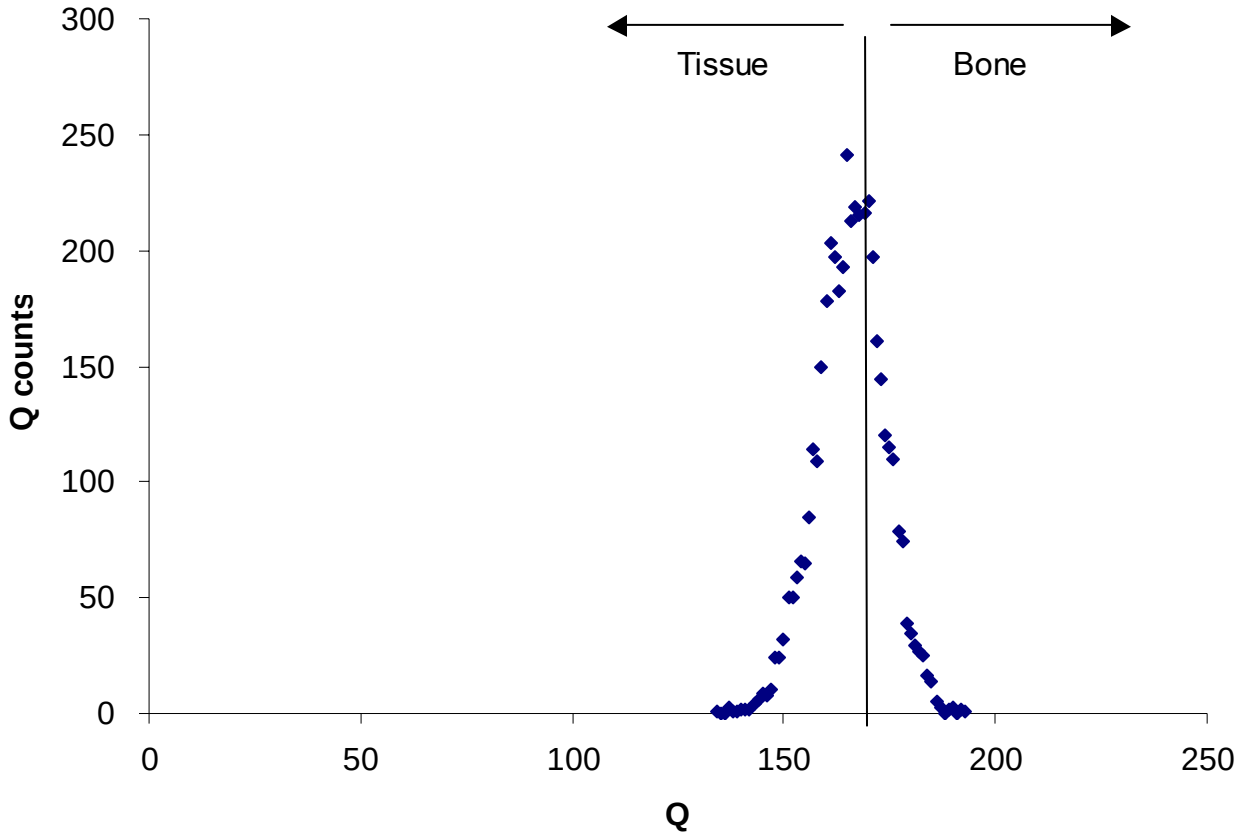

Figure 59. Histogram of the 2nd day region aluminum scan for the pig femur specimen #2.

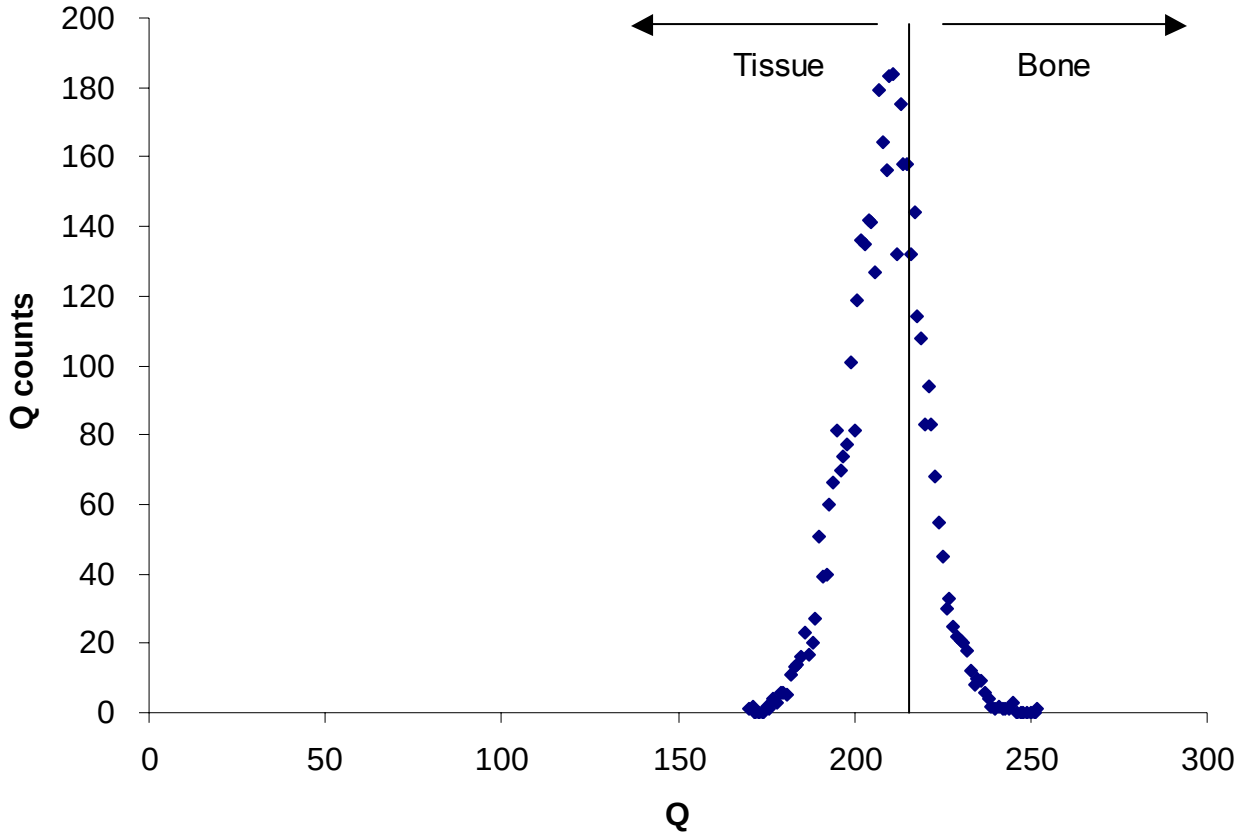

Figure 60. Histogram of the 2nd day region plexiglass scan for the pig femur specimen #2.

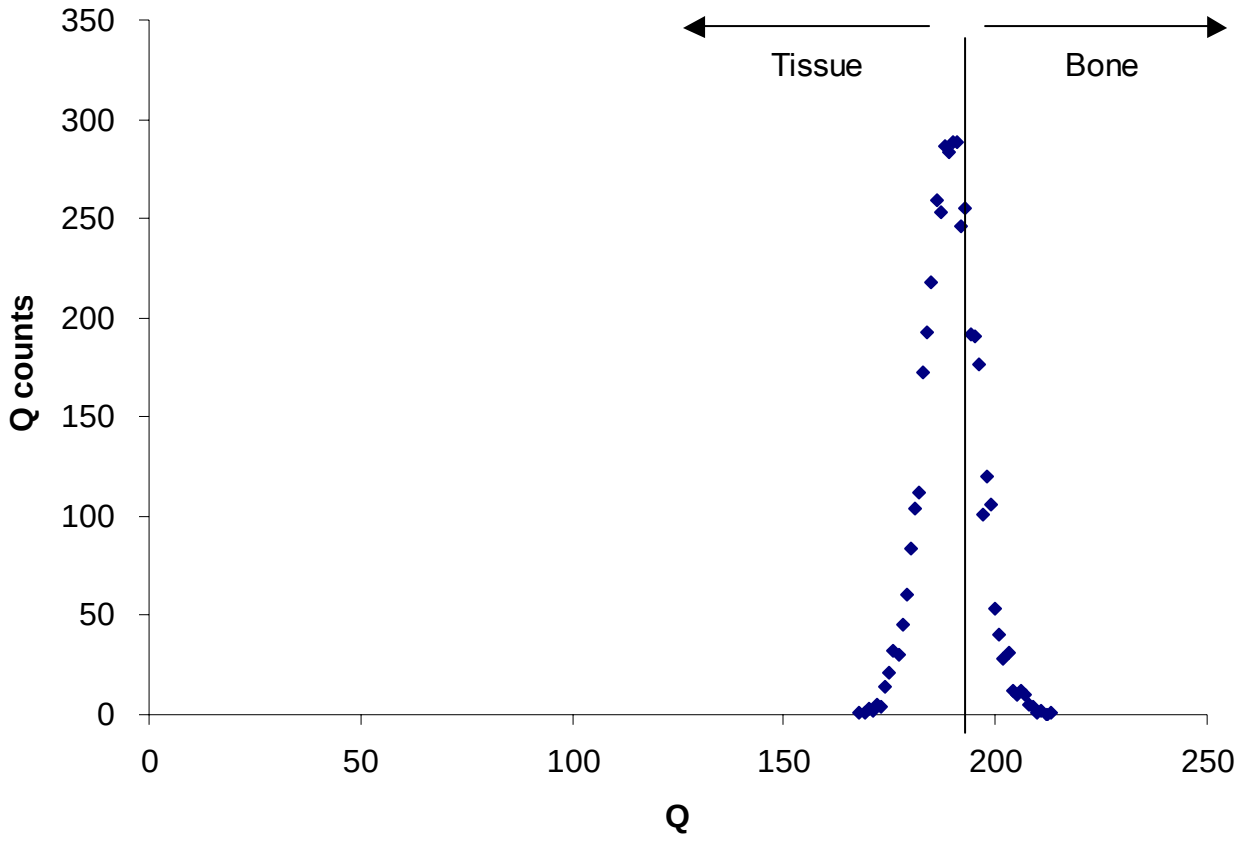

Figure 61. Histogram of the 2nd day region plaster scan for the pig femur specimen #2.

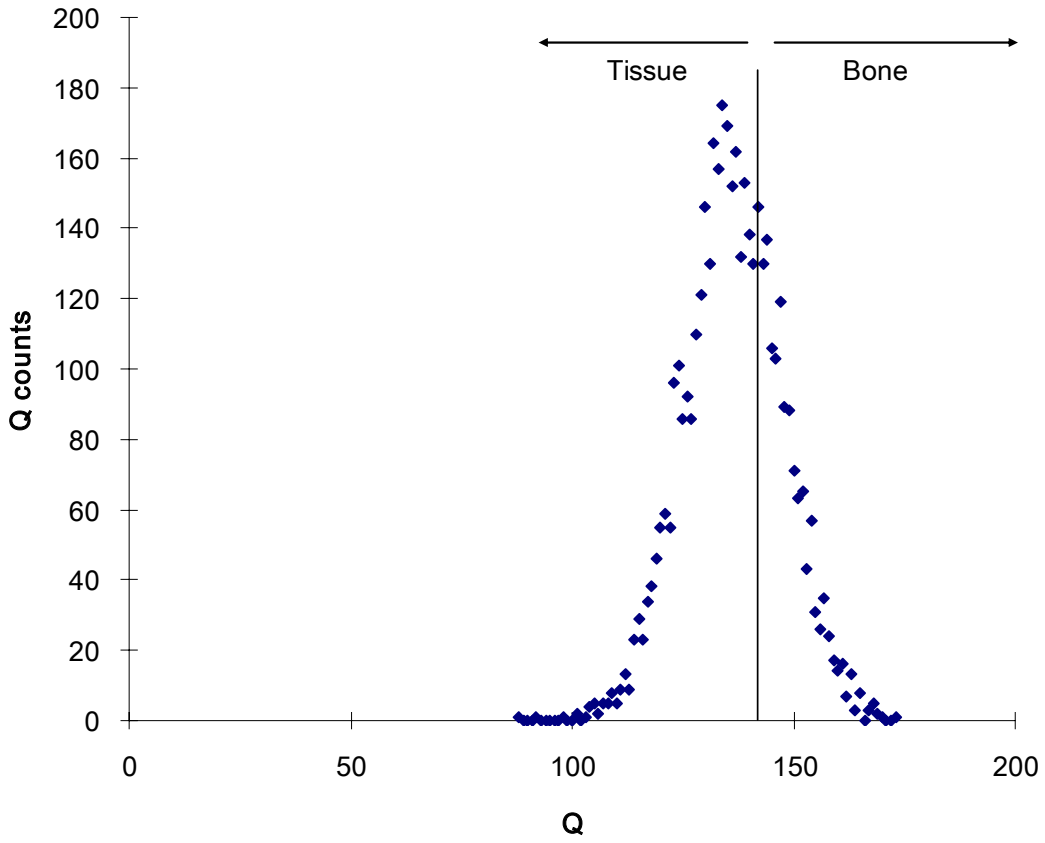

Figure 62. Histogram of the 3rd day region air scan for the pig femur specimen #2.

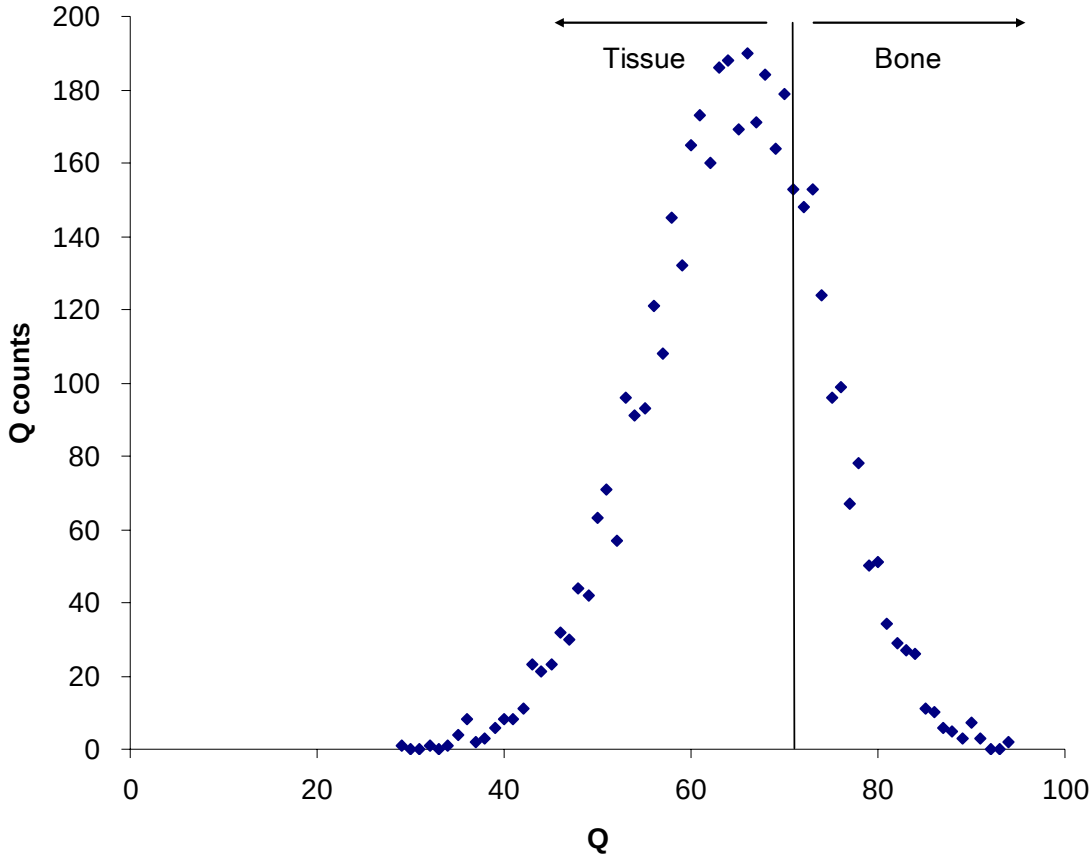

Figure 63. Histogram of the 3rd day region aluminum scan for the pig femur specimen #2.

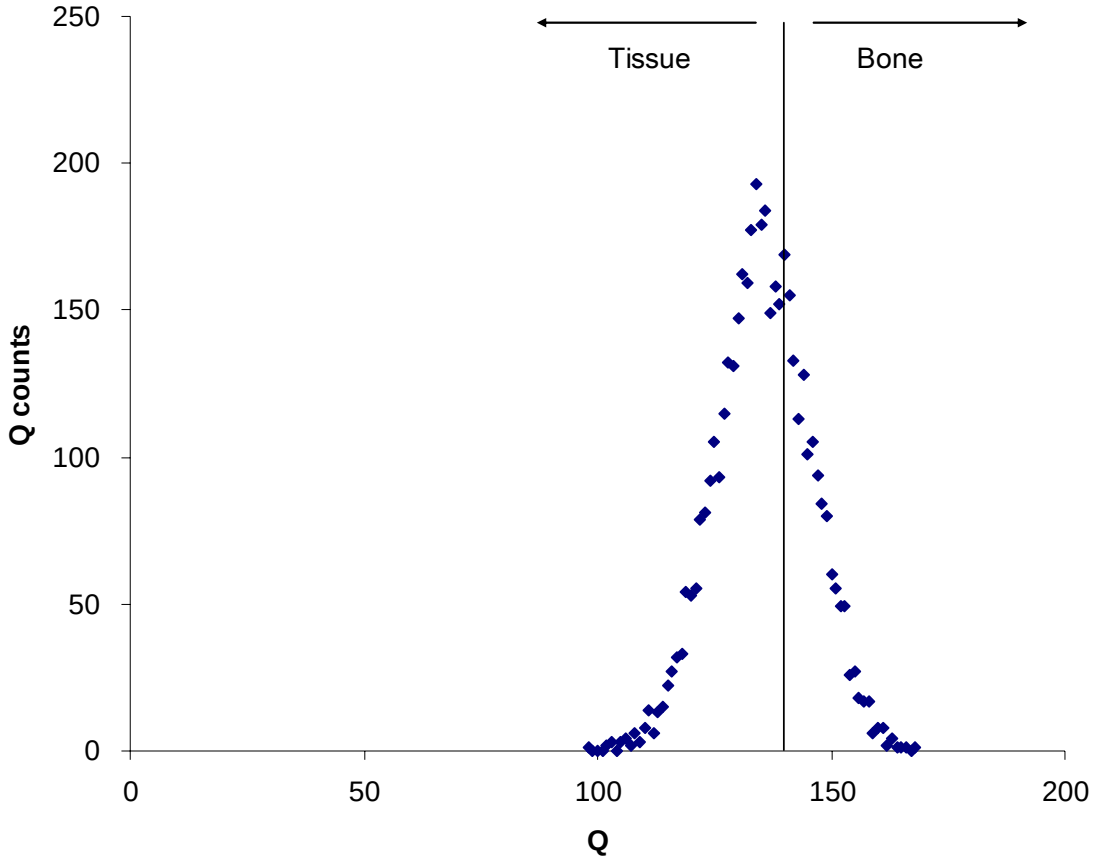

Figure 64. Histogram of the 3rd day region plexiglass scan for the pig femur specimen #2.

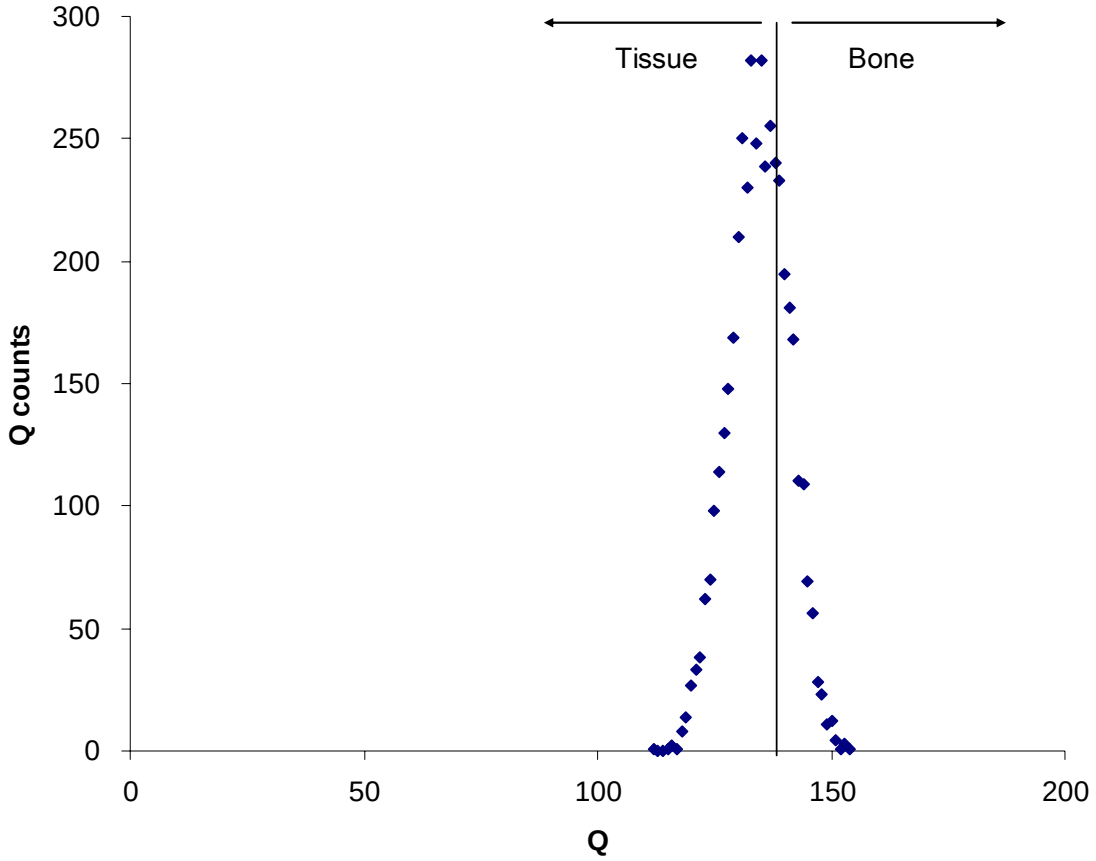

Figure 65. Histogram of the 3rd day region plaster scan for the pig femur specimen #2.

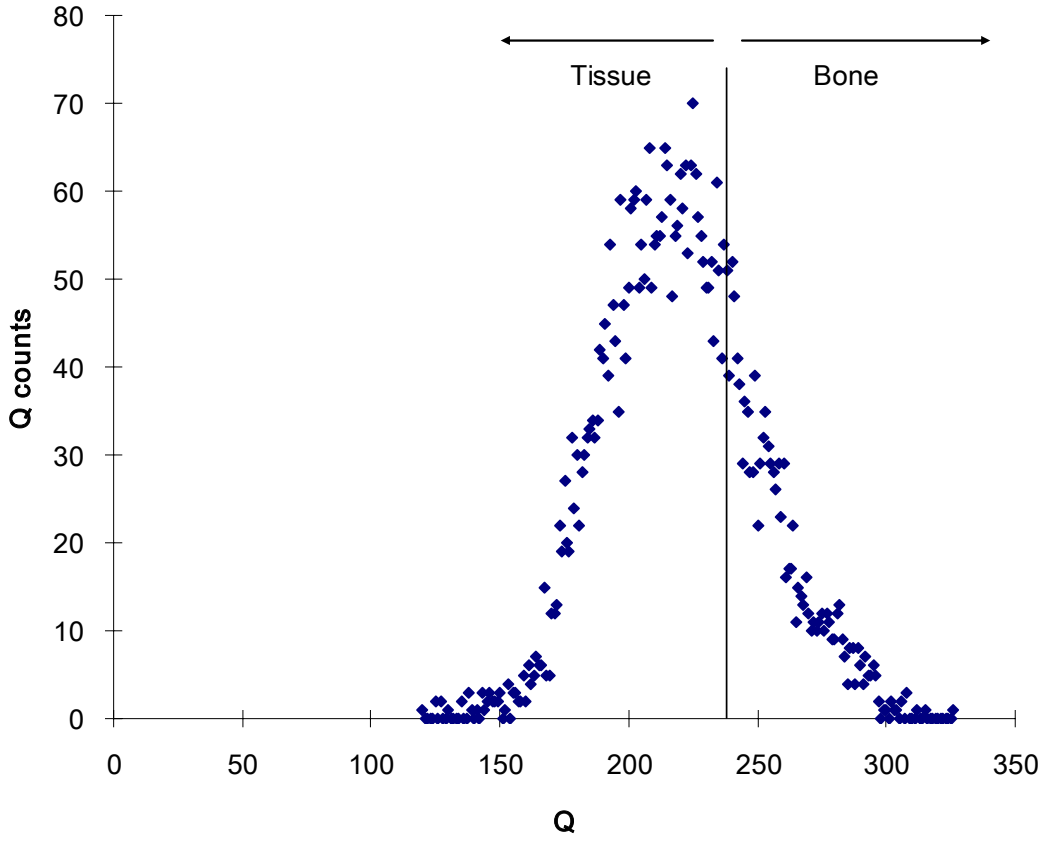

Figure 66. Histogram of the proximal region air scan for the pig femur specimen #2 cut in half.

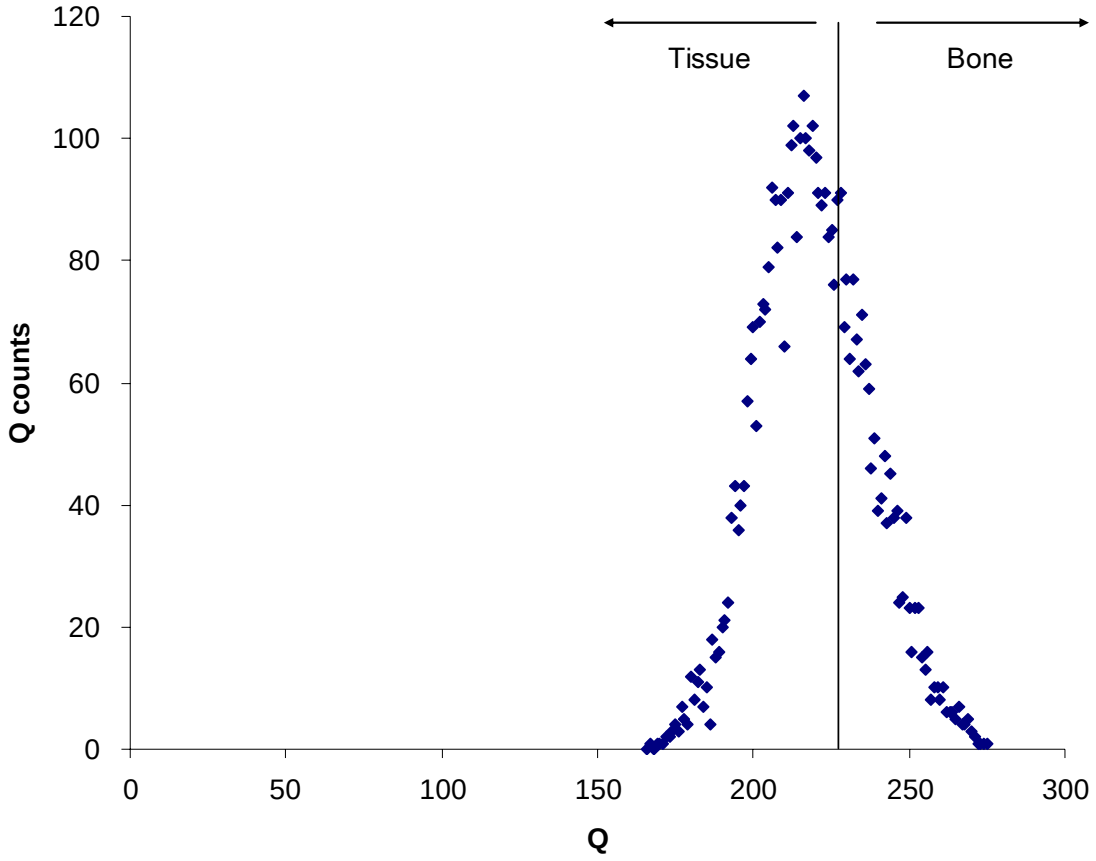

Figure 67. Histogram of the proximal region aluminum scan for the pig femur specimen #2 cut in half.

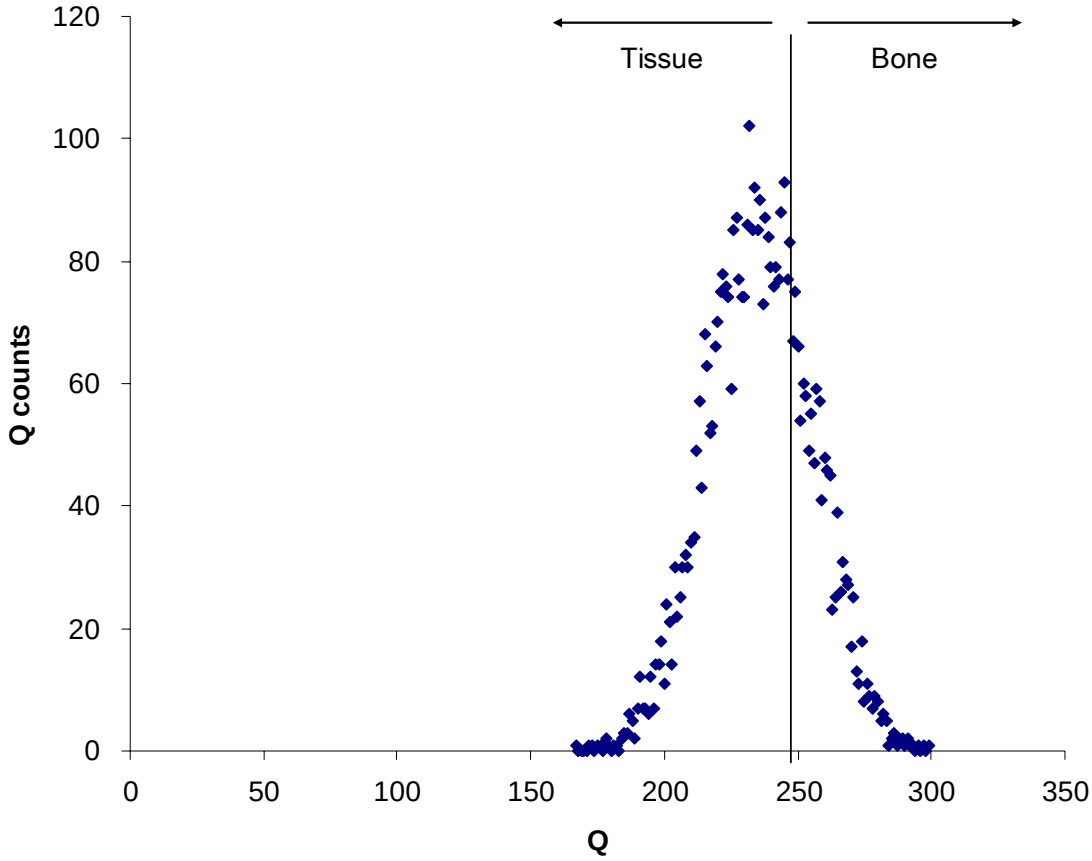

Figure 68. Histogram of the proximal region plexiglass scan for the pig femur specimen #2 cut in half.

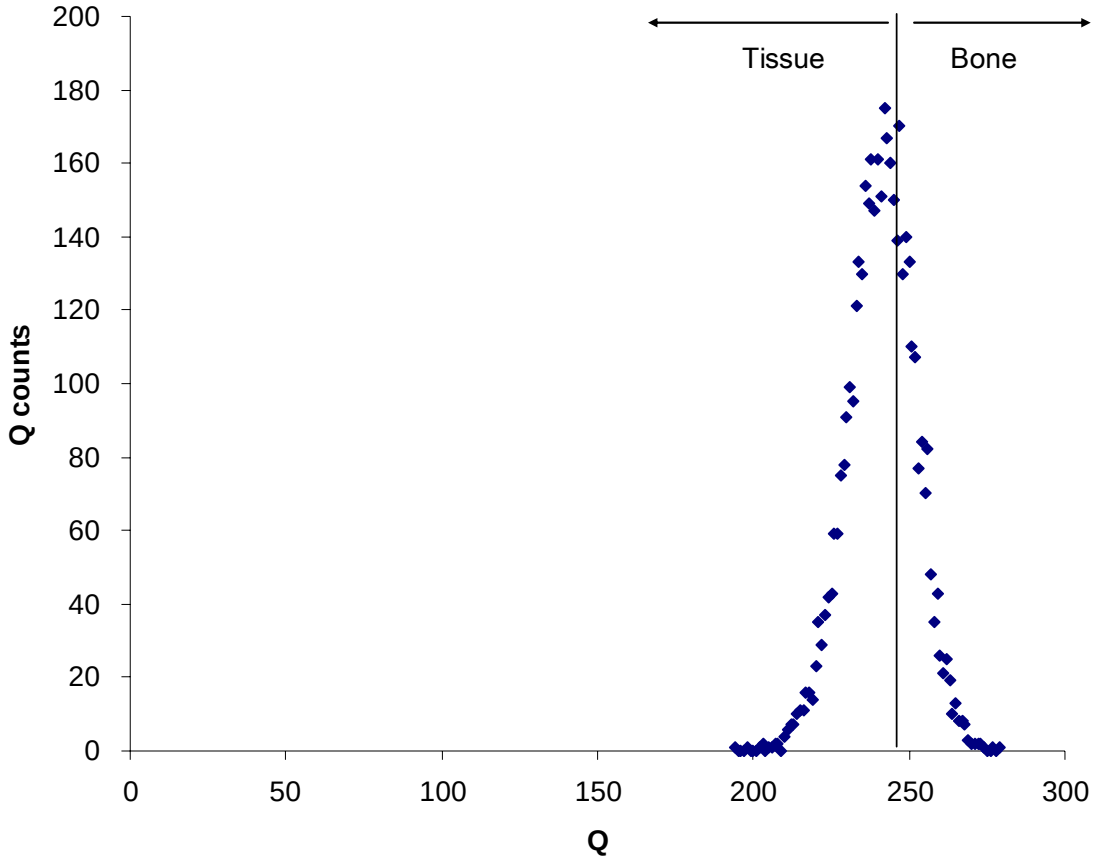

Figure 69. Histogram of the proximal region plaster scan for the pig femur specimen #2 cut in half.

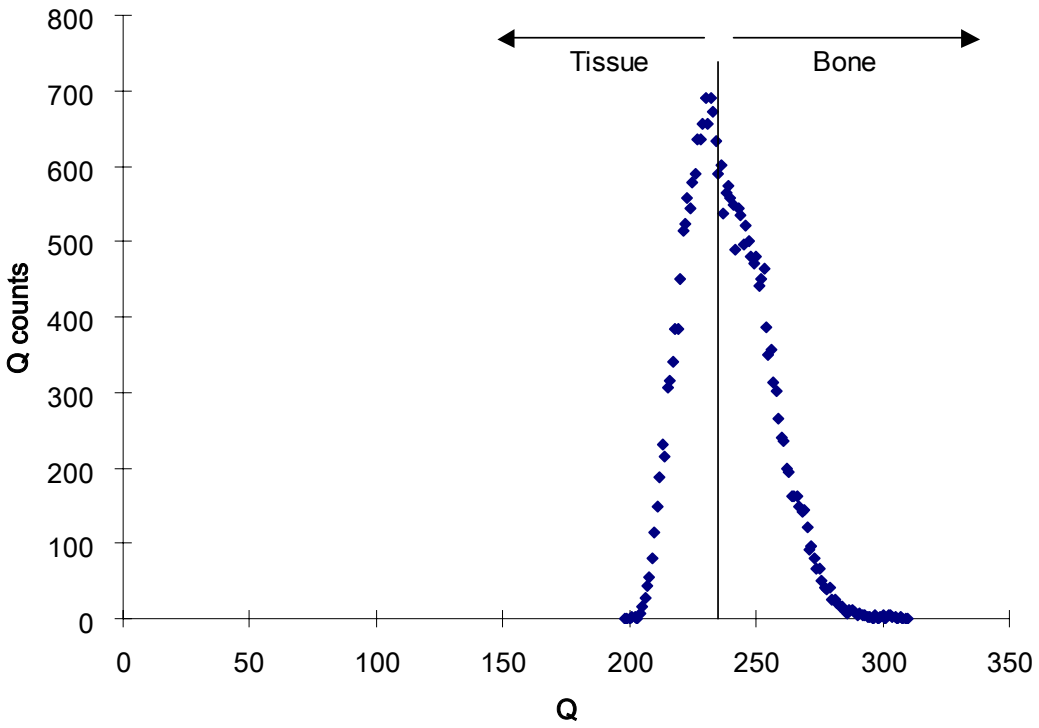

Figure 70. Histogram of the distal end region air scan for the pig femur specimen #2.

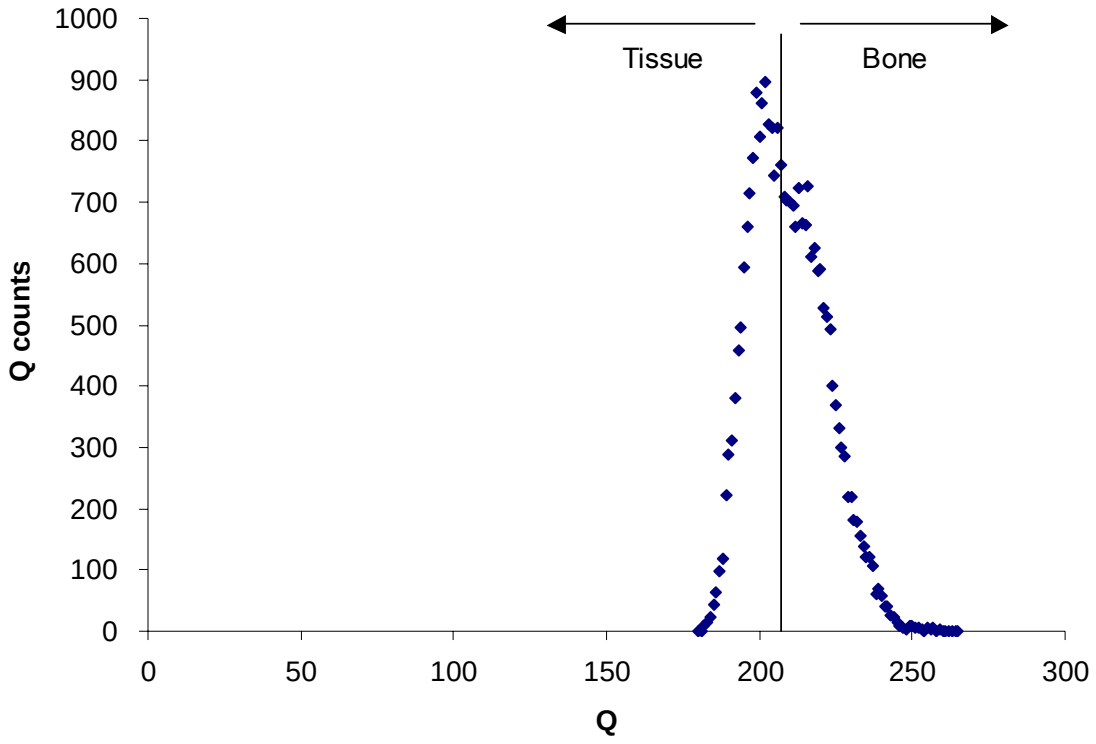

Figure 71. Histogram of the distal end region aluminum scan for the pig femur specimen #2.

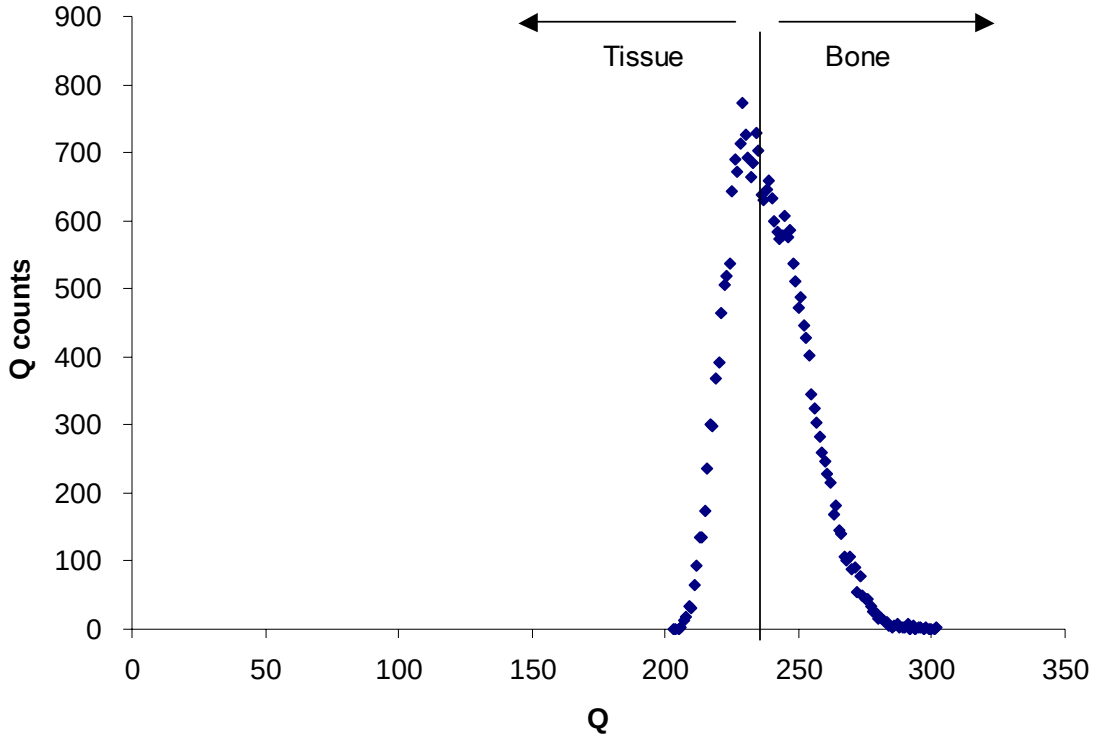

Figure 72. Histogram of the distal end region plexiglass scan for the pig femur specimen #2.

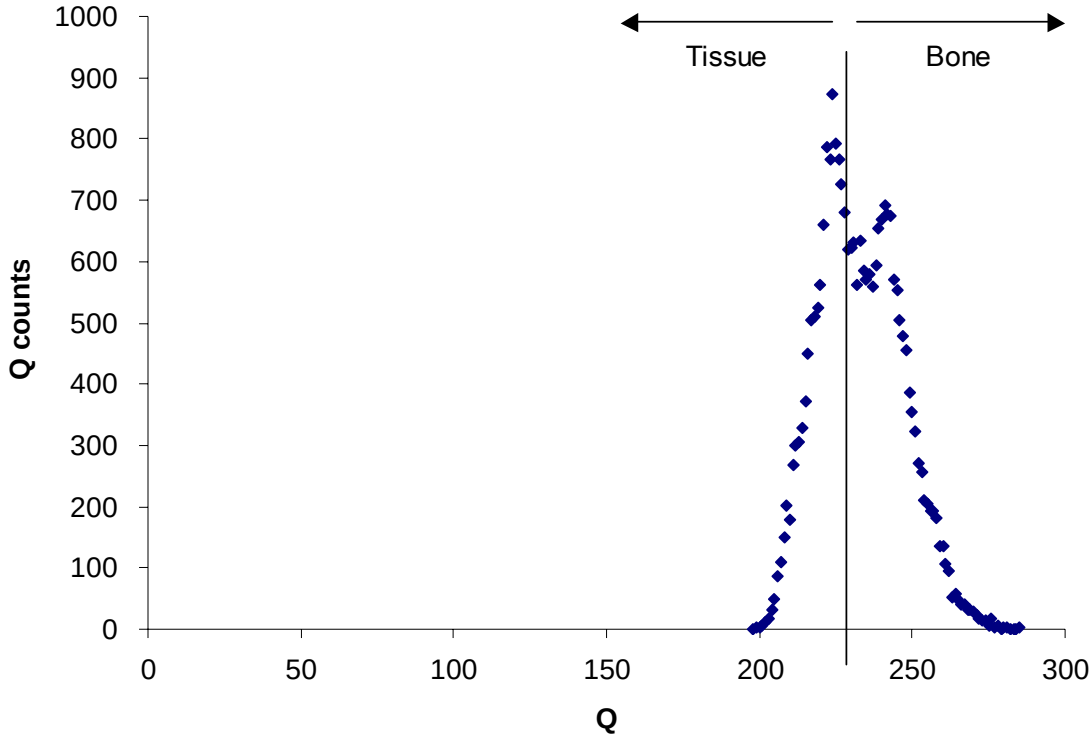

Figure 73. Histogram of the distal end region plaster scan for the pig femur specimen #2.

X. VITA

James Bryant May was born September 25th 1981 in Cincinnati, Ohio. James has lived in Louisville since 1991. He attended Louisville Male High School for all four year. James earned a spot on the freshman and junior varsity basketball teams his freshman and sophomore year. He later joined the cross country and track teams the remaining years of his high school education. He won a state title in track as well as being the team captain for both the track and cross country teams his senior year. He helped lead his cross country team to its highest school finish ever. James enjoys hobbies such as photography and all other sports. He enjoys traveling to our nations national parks and photographing its mystique. He enjoys everything that the outdoors has to offer and loves all regions of the country that he has visited.